ELECTRICAL AND COMPUTER ENGINEERING
DEPARTMENT

CLEMSON UNIVERSITY

CLEMSON, SC 29634-0915

FINAL

TR-080594-4871F

IN-03-CR
NGT-50975
44393
P 80

CHARACTERIZING THE WAKE VORTEX SIGNATURE FOR AN ACTIVE LINE OF SIGHT REMOTE SENSOR

by

Robert Milton Heil

Radar Systems Laboratory
Technical Report No. 19

Characterizing The Wake Vortex Signature For An Active Line Of Sight Remote Sensor

by

Robert Milton Heil

Technical Report #19
August 5, 1994

Radar Systems Laboratory
Electrical and Computer Engineering Department
Clemson University
Clemson, SC 29634-0915

Windshear Detection Radar Signal Processing Studies
Grant NGT-50975
National Aeronautics and Space Administration
Langley Research Center
Hampton, VA 23665

ABSTRACT

A recurring phenomenon, described as a wake vortex, develops as an aircraft approaches the runway to land. As the aircraft moves along the runway, each of the wing tips generate a spiraling and expanding cone of air. During the lifetime of this turbulent event, conditions exist over the runway which can be hazardous to following aircraft, particularly when a small aircraft is following a large aircraft. Left to themselves, these twin vortex patterns will converge toward each other near the center of the runway, harmlessly dissipating through interaction with each other or by contact with the ground. Unfortunately, the time necessary to disperse the vortex is often not predictable, and at busy airports can severely impact terminal area productivity. Rudimentary methods of avoidance are in place. Generally, time delays between landing aircraft are based on what is required to protect a small aircraft. Existing ambient wind conditions can complicate the situation.

Reliable detection and tracking of a wake vortex hazard is a major technical problem which can significantly impact runway productivity. Landing minimums could be determined on the basis of the actual hazard rather than imposed on the basis of a worst case scenario. This work focuses on using a windfield description of a wake vortex to generate line-of-sight Doppler velocity truth data appropriate to an arbitrarily located active sensor such as a high resolution radar or lidar. The goal is to isolate a range Doppler signature of the vortex phenomenon that can be used to improve detection. Results are presented based on use of a simplified model of a wake vortex pattern. However, it is important to note that the method of analysis can easily be applied to any vortex model used to generate a windfield snapshot. Results involving several scan strategies are shown for a point sensor with a range resolution of 1 to 4 meters. Vortex signatures presented appear to offer potential for detection and tracking.

ACKNOWLEDGMENTS

The author wishes to express heartfelt appreciation to all who have contributed to the following work. My Father above, first and foremost, deserves all of the praise and glory for the insights this work have brought and to the significant increase in patience this work has caused to the author. A month before a thesis comes due might not be the best time to pray for more patience.

The Masters Degree committee members, Dr. John Gowdy, Dr. Robert Snelsire, Dr. John Komo, and most of all Dr. Ernest G. Baxa Jr. have been instrumental in accomplishing this work. Dr. Baxa has also provided abundant guidance and support to a young man struggling to unravel his future. Dr. Baxa provided pathways which enabled NASA Langley Research Center to fund and support this effort, and thanks to their team is also given.

The author wishes to thank his family, especially his wife Cynthia, for their encouragement, support and gift of fueling his desire to always learn more. As a teacher, countless other students have briefly touched his life, and brought uplifting words of encouragement with uncanny timing. Thanks, lastly, go to Clemson University, for shaping his best years, so far, and providing a chance to leave this world a better place for his having been here. "Within each man lies the rough, uncut materials that, when shaped and polished by effort and desire, produce the most brilliant and sought after Diamonds."

TABLE OF CONTENTS

LIST OF FIGURES

List of Figures (Continued)

Page

CHAPTER 1
INTRODUCTION

Terminal area productivity remains a problem for larger airports, due in part to the threat of aircraft induced turbulent wind patterns. Safety concerns call for a time delay between landing planes to minimize these dangerous encounters, but these unused "windows" adversely affects landing/take-off productivity. At the present time, there are no remote sensor means employed to detect these events, and air traffic controller generally use enforced time delays. However, ongoing research exists to address detection of wingtip induced, air hazards called wake or tip vortices using a remote sensor.

One type of sensor being investigated is a pulse Doppler radar. Radar is a commonly used word in today's aeronautical technology. However, recent success in the on-board windshear detection systems [1, 2, 3], show that the extent to which radar can assist a pilot, especially during a take-off or landing, is still growing. Two distinct methods of implementing radar exist. The first method works on a continuous wave (CW) emission but requires a separate receiver [4]. Since there are no breaks in the wave transmission, the system cannot estimate range to target without some modulation. In a pulsed wave system, however, the same antenna is used to transmit and receive the signal, as illustrated in Figure 1.1. Basically, a pulse of electromagnetic energy is released from the system, and then the system switches to a receiving mode. This design can be viewed as a modulated CW that will satisfy the range to target concerns. As the energy encounters reflective particles, often called targets [4], an echo signal is returned to the system. Examination of this signal can yield valuable information about the target, including location and range, velocity, and even size.

Another sensor under investigation, is lidar. A more recently developed technology which involves pulsing a laser operating at light frequencies, lidar seems a likely

candidate because of the finer resolution available. With an appropriate receiver and through signal processing, such a system is very much like a pulsed Doppler radar with the potential for much higher range resolution. This work assumes use of a pulsed wave sensor to develop a line-of-sight (LOS) relative windspeed spatial pattern signature of a wake vortex. This will be based on an assumed aerosol-type reflectivity return.

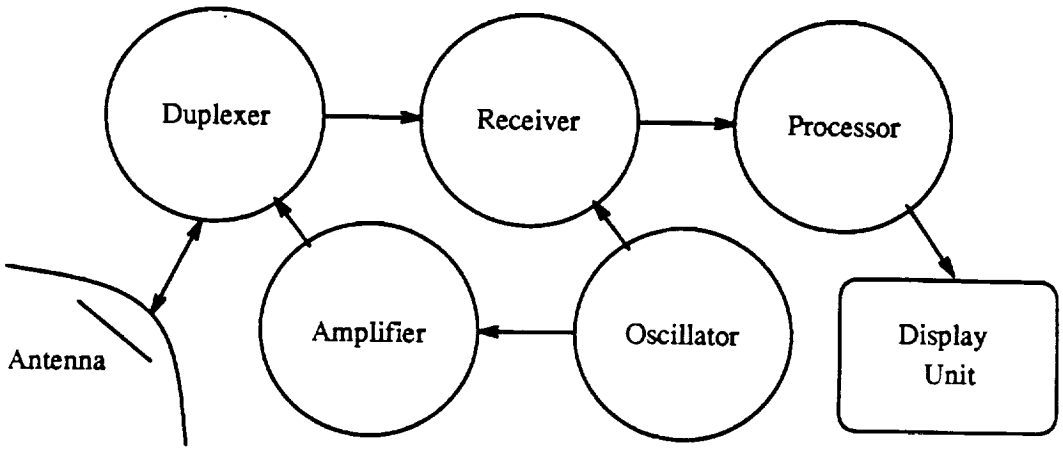

Figure 1.1 Pulse wave radar system in block form.

1.1 Vortex Definition

A vortex is a common phenomenon in science. A simple model can be made by connecting two plastic soda bottles together, one empty and the other one full. The result would appear similar to an hourglass timer. When the full bottle is placed above the empty one, and the water is allowed to drain down, a liquid version of a vortex will naturally form. The vortex also forms when a drop of water falls into a laminar plane of water that is much deeper than the drop's length [5]. One can view a vortex by looking at the end of a conch shell. The ever-increasing (or decreasing, depending on your view point) spiral can describe this pattern, see Figure 1.2. Unfortunately, there are some man-made examples of a vortex that are neither visible nor desirable under certain circumstances. Vehicles of all kinds produce these air turbulences. Bicycles,

automobiles or trucks, naval aircraft carriers and submarines, and even airplanes, generate these induced flows that are natural products of mass in motion [6, 7].

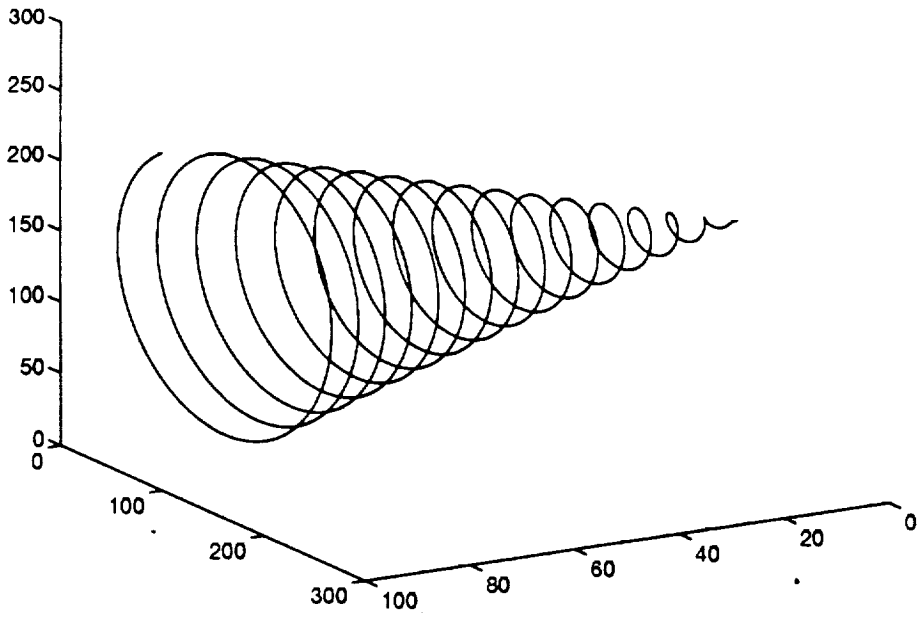

Figure 1.2 Vortex pattern developed by $t * sin(t)$ and $t * cos(t)$.

There are also numerous and successful attempts to model the vortex [8, 9]. An important factor used in discussion and calculation of the vortex is the Reynolds Number R defined by

$$R = vd/\nu \tag{1.1}$$

where v indicates the stream velocity, d is the typically the diameter or other similar linear dimension, and ν is the kinematic viscosity defined as $\nu = \mu/\rho$, with μ as the viscosity and ρ as the density of the medium. A thorough explanation of the development of the Reynolds Number can be found in the work by Garrett Birkhoff [5]. As R increases, the model of flow undergoes well defined and empirically duplicated metamorphoses [5, 10].

For $R < 0.1$, the stream is commonly defined as a "creeping flow," and will exhibit well defined symmetry. Mushroom spores and tree pollen have an estimated

R value of 0.001 to 0.01 respectively. Small organisms, such as bacteria and protozoa, have a 10^{-6} to a 10^{-3} Reynolds number and use friction forces to propel themselves [6]. As R increases to around 5, streamlines will develop behind the object, destroying true symmetry. From 5 to 25, however, two stationary vortices may form behind a cylindrical or spherical object, and a more well defined single vortex behind an "arm" or wing becomes evident. It is in this range that a well defined laminar "boundary layer" of concentrated vorticity forms along the body of the vortex [5]. Any organism (or in this case machine) that has a larger than unity Reynolds Number propels itself inertially [6].

As R continues to increase, up to around 1500, multiple, random flows become more and more frequent, and vortices are shed from the main vortex periodically. For R above 1500, periodicities become harder to detect, and the flow becomes increasingly turbulent. Section 2.2 covers more information on the use of the Reynolds number in this work.

1.2 Wake Vortex Generation by Aircraft

The airplane, as well as all flying animals, generates a vortex naturally. As the aircraft begins to move forward, a series of events occur, studied by Lanchester and later by Prandtl in the early to mid-1900s [6], that will produce lift. Air encountering a "wing" placed at an oblique angle will flow over the wing more quickly than under it. This flow generates a low pressure area above the wing and a high pressure area below the wing. The wing then tends to move toward the low pressure area, causing lift. However, the air passing under the wing begins to spiral downward as a result. Figure 1.3 shows the results of Prandtl's studies. These results are formulated mathematically by Kutta and show that the sum of clockwise force in the bound vortex equals the negative force found in the mobile starting vortex. It is the tip vortices that cause the most concern during takeoff and landing.

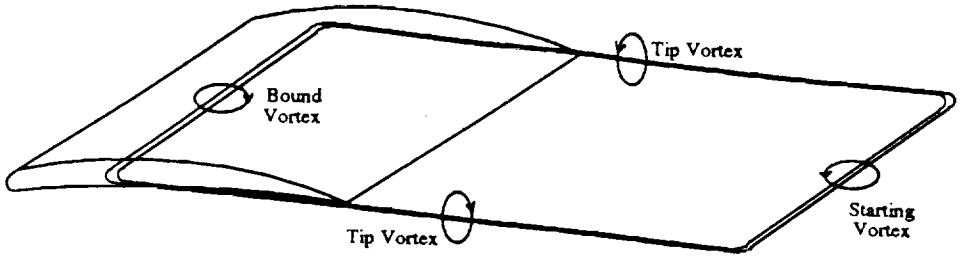

Figure 1.3 The closed vortex ring, by Prandtl.

As shown by Figure 1.4, the tips of the wings (and to a lesser degree the tips of the tail wings) are the point of generation of a closely matched pair of vortex patterns termed a "wake vortex." As the air moves past the wing tips, the aerodynamics of lift cause a spiral-like effect to the surrounding air. The result is much like taking that conch shell and stretching it out over a much larger area for each wing tip. The wake vortex is strongest and smallest at the tip of the wing, and as the aircraft moves past, this spiral expands and weakens until the existing wind conditions reassert themselves. As expected, the strength of the wake vortex is directly dependent to the mass of the aircraft. So a larger plane will generate a bigger, longer lasting, and stronger vortex than a small plane.

Public interest in these air disturbances is also growing. Science and aeronautical periodicals cite these phenomenon and how one may attempt avoidance during aircraft flight [11]. Garrett Birkhoff even ties in the existence of these vortex "flows" to the evolution of many aquatic and plant life [5]. *Discover* writer Steven Vogel describes the properties of vortex flow and generation using nature and her animals as examples [7]. The Research Triangle Institute (RTI) and Georgia Tech Research Institute (GTRI) performed a study for NASA (NAS1-18925) to explore civil aviation atmospheric hazards. Part of their work focused on the occurrence of the aircraft induced wake vortex hazard, the impact on aviation, the possible measurables, and the feasibility of active or passive techniques [9]. A common theme across the existing information,

is that the current measures of avoidance during an airplane landing or takeoff are barely sufficient at best.

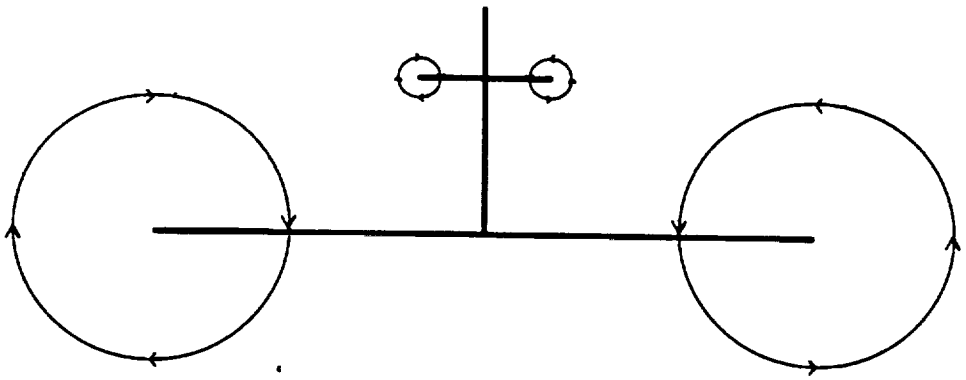

Figure 1.4 Trailing view of aircraft generating a wake vortex.

1.3 Runway Hazards

Generating a wake vortex poses no problems to the aircraft responsible. However, to the next landing plane, intense vortex conditions have resulted in fatalities, injuries, and aircraft damage [9, 11]. Since the mass of the first plane influences the degree of the vortex, a severe case would involve a large plane followed by a smaller one. The first plane creates the twin vortex as it lands. In a minimal crosswind situation, each wake vortex cone will expand and actually "roll" toward the center of the runway, dissipating harmlessly when they collide with the ground or each other. Sixty-nine percent of the reported vortex encounters have occurred during final approach or landing, and nineteen percent during takeoff [9].

When a crosswind does exist with enough force to push the vortex opposite to its normal path, typically between three and five knots [9], one of the cones may become positioned directly in front of the next landing craft. If the wingspan of this second aircraft encounters the invisible spiral of air, rotation of the aircraft can occur. In fact, when large transports (150,000 to 300,000 lbs.) are the generating aircraft, 30 to 60 degree rolls are typical [9]. Some planes have had wingtips to hit the runway, while

others have had landing gear, propeller, and landing lights damaged from runway contact. A few pilots have even found themselves completely inverted during final approach. These severe (70 to 180 degree) rolls almost always involve a small aircraft (less than 5000 lbs.), a small transport (5,000 to 14,500 lbs.), or a medium transport (14,500 to 30,000 lbs.), that is following a wide body (greater than 300,000 lbs) [9].

A secondary problem occurs when there are parallel runways. The first plane generates a vortex that begins to spiral away from the original landing strip. Unfortunately, one of the cones may drift into the adjacent runway, posing a threat to aircraft landing there. This can happen both in still air, as well as a crosswind. A recent holiday crash involving a Westwind jet in Orange County, California has received attention because the NTSB investigators have been pointing to wake vortex turbulence as the probable cause of the accident that claimed the lives of all the passengers [11].

1.4 Existing Precautions when Landing

When an aircraft lands, there are existing precautions in place to help reduce the possibility that the next landing aircraft will not encounter a vortex. The standard means of avoiding a vortex involves imposing landing separation time minimums. It is the job of the air traffic controller to inform a landing pilot what size plane has preceded him, and to allow "sufficient" time to elapse before granting runway approach clearance [11]. As the ratio between first and second aircraft size increases, so does the time limit between landing attempts. So if a small plane lands behind a large plane, there is a greater time delay to allow any wake vortex patterns to weaken and dissipate. In addition, these safety minimums will be increased if there is a crosswind that would enhance the hazard.

Another intuitive method adopted by pilots involves altering their final approach path. By adjusting the entry angle, a pilot can safely land by flying over the peaks of any vortices still on the runway, as shown in Figure 1.5. The vortex generating

airplane approaches on slope a. The second pilot adjusts his slope to $a + b$ to avoid the vortex. However, if the third landing pilot adjusts his entry by the same amount as the second landing pilot, the original problem returns.

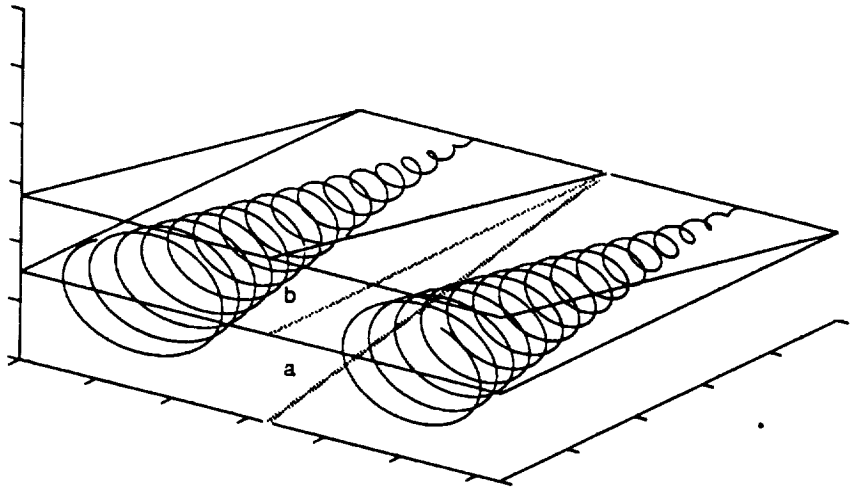

Figure 1.5 How pilots modify their approach slope.

1.5 Problem Statement

This work relates to the use of a pulse Doppler radar or lidar to detect the occurrence of the wake vortex phenomenon. A simplified model with general assumptions has been developed to assist in this work. Scaling effects and dynamic expansion of the vortex are explored, and a "signature" for aerosol-filled airspace returns is computed. Finally, an attempt is made to evaluate the feasibility of high resolution radar and lidar systems as a means of detection.

Chapter 2 explains the windfield development, sensor placements, and the importance of the scan angle variation. Chapter 3 presents various simulations and their results. Effects of range resolution on signature clarity is discussed. Chapter 4 makes concluding remarks and suggests possible avenues for further development.

CHAPTER 2

MODELING THE WAKE VORTEX

There are many sources currently attempting to model the wake vortex phenomenon so that detection and tracking through remote sensing may one day become a reality. However, there are as yet no accurate mathematical models that can represent the three-dimensional, aircraft induced wake vortex situation [9]. This work has involved developing a representation of an airspace volume surrounding a generic airport runway so that a wake vortex airflow pattern can be inserted as a set of sampled windspeed vectors positioned throughout the volume. The model enables evaluation of line-of-sight (LOS) wind speeds relative to a fixed point about the runway, characteristic of what might be observed with a high resolution pulse Doppler radar or lidar system used to illuminate such an aerosol filled flow field. The wake vortex is represented as a series of two-dimensional rings of turbulent flow that make up a conical pair of vortex-like airflow patterns. Although suitable radar or lidar systems with a one to two meter range resolution are not yet available, it is of interest to determine LOS truth data descriptions of these phenomena which can be used to define a wake vortex range-velocity signature. It is believed that this type analysis can have several purposes including evaluation of the usefulness of a high resolution LOS sensor, the investigation of the best vantage point for such a remote sensor in terms of the "radar signature", and ultimately to improve the ability to detect and track these events.

2.1 Volume Definition

To establish the air flow field, certain compromises had to be weighed. A runway can be 50 to 70 times longer than it is wide (Orlando International, for example, has one runway 10,000' by 150' and two runways 12,000' by 200' [12]). Furthermore, trailing wake vortex patterns have been documented as far as six miles behind the

aircraft [9]. Another complication pertains to the aircraft itself. As an airplane begins its final approach, the vortex patterns are in their cleanest and simplest form. However, when the flaps are lowered, two conditions develop. The vortex flow tends to decrease in severity as a result of the introduced flaps, but the flaps also generate new, multiple wake vortex pairs and increase the shedding of the existing vortex cones. So the closer an aircraft gets to completing the landing event, the more complex and less understood the wake vortex problem becomes [11].

The spatial resolution of the windfield vectors is the other major factor to consider. An airspace volume divided into 1 m cells, each containing three windspeed components, would require approximately 118 million data points for a 10,000' by 150' runway calculated to a height of 100'. Considering the symmetry of a simple vortex, viewing a smaller portion of the event should be sufficient. Therefore, the analysis has been set up to view a portion of the runway airspace into which an expanding vortex pattern is inserted for evaluation, as illustrated in Figure 2.1. This reduction of the airstrip volume greatly decreases the bulk of data necessary for each flight simulation of the model, but still enables a very high resolution analysis of the vortex phenomenon.

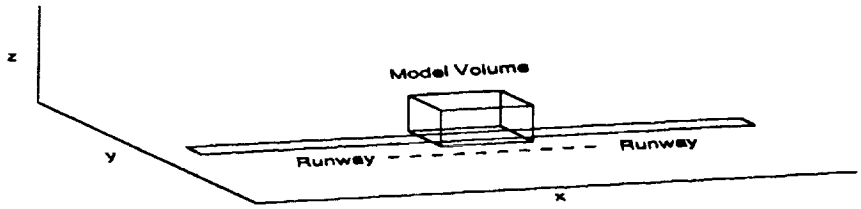

Figure 2.1 Volume definition about a generic runway.

The resulting volume of space around the runway was set to 400 meters along the runway length, and 100 meters along the runway's width and height, as indicated

in Figure 2.2. The.coordinate system sets the negative x-axis along the path of the plane, the y-axis across the wings of the plane, and the z-axis to indicate height. The volume origin point is to the left, and in front of the landing aircraft.

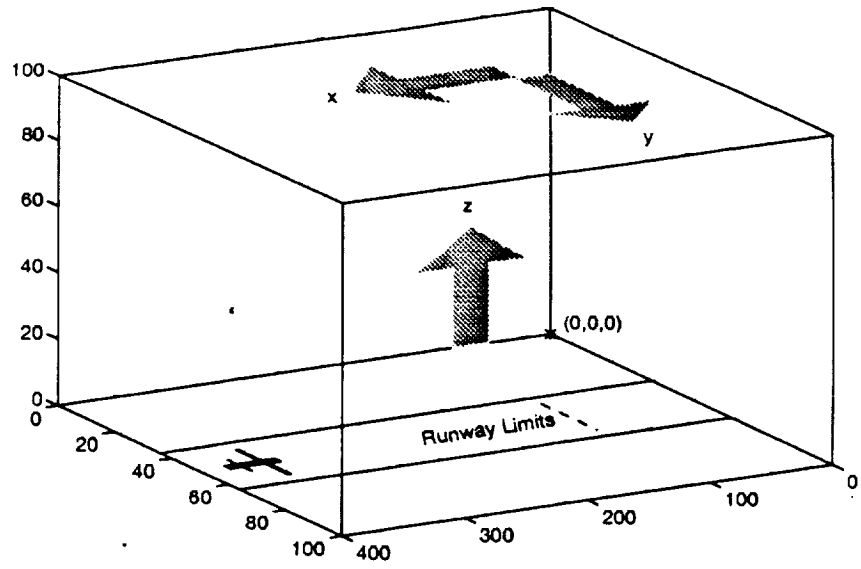

Figure 2.2 XYZ volume and coordinate system of model.

The volume is subdivided into small cells that contain windspeed information, as shown in Figure 2.3. The model parameter that controls this cell size is the *spacing* parameter. A *spacing* of 1 would indicate a cell of one cubic meter (1x1x1). Similarly, if the *spacing* were increased to 4, each cell would represent 64 cubic meters (4x4x4). For a volume size of 400 by 100 by 100, and a *spacing* of 1, there would exist 4 million cells. The *spacing* in the simulations ranged from 1 to 4 meters. Each cell contains a three component windspeed determined from the windfield description as an average windspeed in each axis direction over the specified elemental volume spacing which is stored in vector form. The model then calculates component windspeed vectors for each vortex cone using the exponentially expanding rings as the basis. It should be noted that any wake vortex windfield model can be used. All that is needed is a snapshot of the windfield as input to this analysis. In this work a two-dimensional ring of increasing size is used. Following is a detailed description of the ring growth.

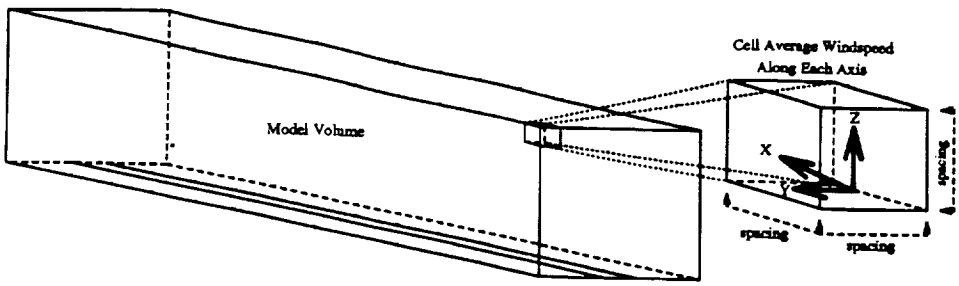

Figure 2.3 Breakdown of the volume into cells of windspeed information.

2.2 Model Parameters

Once the volume has been established, the next step is to insert the wake vortex model information. The model assumes that the aircraft is in its final approach and therefore on a linear and horizontal flight path. The elemental flow field is set up by evaluating the selected volume along successive vertical planes down the length of the runway. These planes are YZ arrays that fit together to form the entire volume. The vortex information is calculated and then inserted into the array. The array values are saved as x, y, and z component arrays to a storage media. For example for x=400 meters and a *spacing* of 1, there would be $x1$, $y1$, and $z1$ to $x400$, $y400$, and $z400$.

To run an analysis, a view point is specified anywhere within or outside the defined volume, and the LOS relative velocities from the center of each elemental volume to that view point is computed. These computed values represent the true LOS relative velocity that could be observed by an ideal directional sensor located at the view point. By taking a vertical slice through the volume, the wind direction can be viewed from the end of the cone. Figure 2.4 depicts such a slice. Note that the left ring is spinning clockwise, while the right ring is counter-clockwise, and that the center of the pair is at a height of 24 meters. Figure 2.5 shows a projection of the wake vortex flow field onto a horizontal plane at a height of 20 meters for an aircraft at a height of 24 meters. The horizontal projection was done at a height of 20 meters so that the horizontal components of each cell could be examined. Note here that a

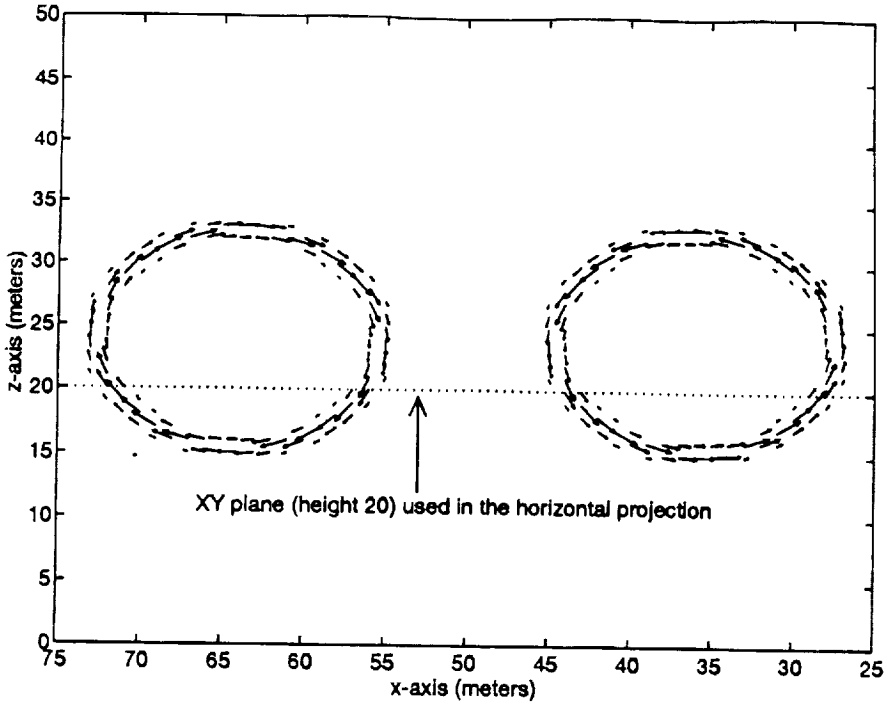

Figure 2.4 Vertical projection at x value of 380 meters.

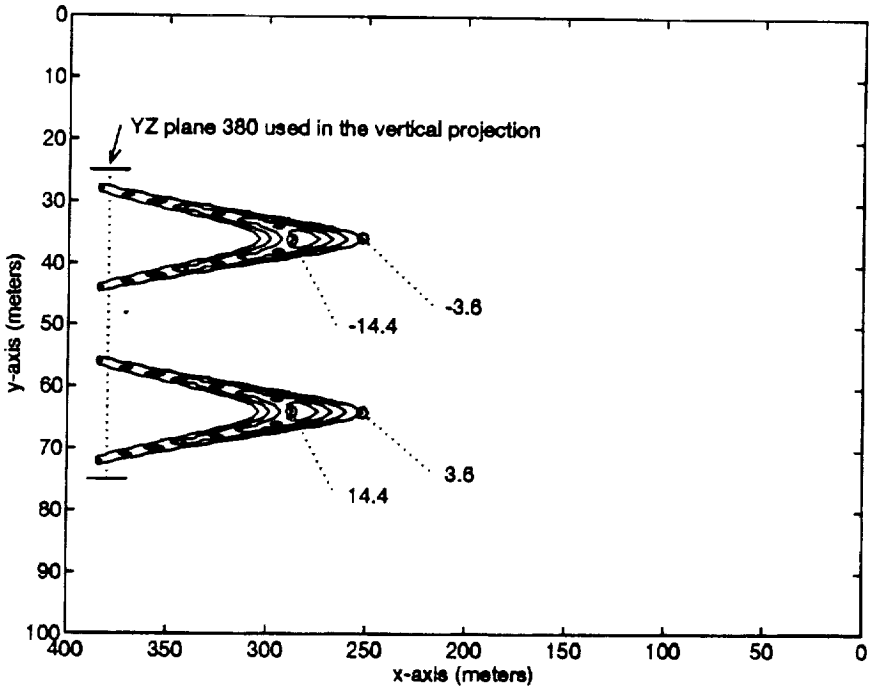

Figure 2.5 Horizontal projection at height of 20 meters.

horizontal "slice" through the exact center would result in an empty set since all of the windspeeds are in a vertical direction at that height. This is discussed in more detail in Section 3.1.

The vortex model uses a set of vertically oriented rings of air flow with an exponentially increasing diameter as the distance from the aircraft increases in the x-axis direction. This is illustrated in Figure 2.6. The model does not generate x-axis windfield components for the vortex rings, but the LOS analysis program utilizes all three directional vectors. This is because, compared to the other components, the x component is much smaller [6], and the contribution of the x component will always be in the negative x direction, since the vortex will flow toward the aircraft as it passes.

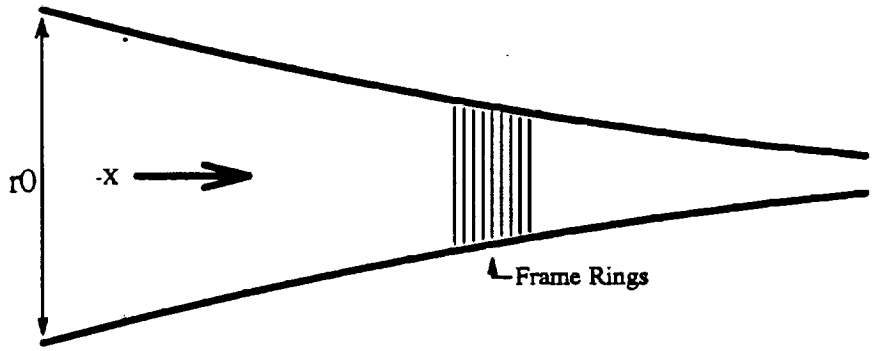

Figure 2.6 Exponential shape of the model.

In Figure 2.4 the left and right vortex are separated by 28 meters from center to center, or roughly 19 meters between the vortex edges. This would fit the dimensions of a medium to large passenger or cargo aircraft (The Boeing 737 has a wingspan of 28.8 meters, and the 747 is 64.4 meters [12]). The study performed by RTI and NASA also indicates that the pair of vortices are typically 1 to 10 meters in diameter, and separated by 75% of the aircraft's wingspan [9]. The aircraft height for the simulations is set to 24 meters above the runway, primarily to insure a wide range of scan angles and sensor placements. The Reynolds number, although not directly

used in this specific model, is intended to fall in the 10^4 or 10^5 range, indicating a very turbulent flow with multiple shedding cones along the wingspan [5, 6].

Two factors determine the magnitude of the windfield cells in the vortex ring. As the vortex ages behind the aircraft, it expands in radius, but weakens in intensity. In assigning a wind vector to a cell, a simple thresholding technique is used to decide whether a cell has a vortex component or not. A threshold value is applied assuming that the windspeed at the nominal ring radius decreases exponentially in a radial direction, as shown in Figure 2.7. The figure shows that the tangential windspeed decreases more rapidly for the smaller rings, and that the rings that are "closer" to the aircraft, have less vectors passing the threshold; but the ones that do pass have a large magnitude. A larger ring that is further behind the aircraft will have more vectors over the threshold, but the maximum windspeed will be smaller. This is illustrated in Figure 2.8 for a vertical ring at 380m behind the aircraft, and for a vertical ring at 180m behind the aircraft. The direction of the non-zero windfield components is then calculated as the tangential angle in the flow direction (clockwise for the left vortex, or counter-clockwise for the right vortex).

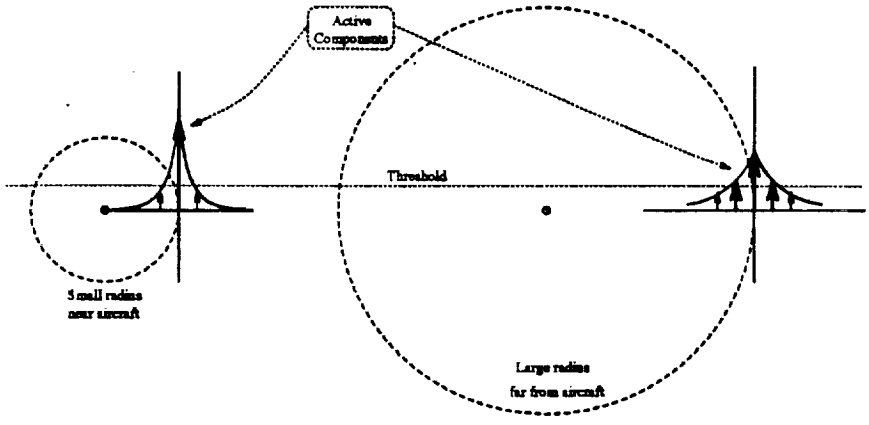

Figure 2.7 YZ threshold of rings with varying radius.

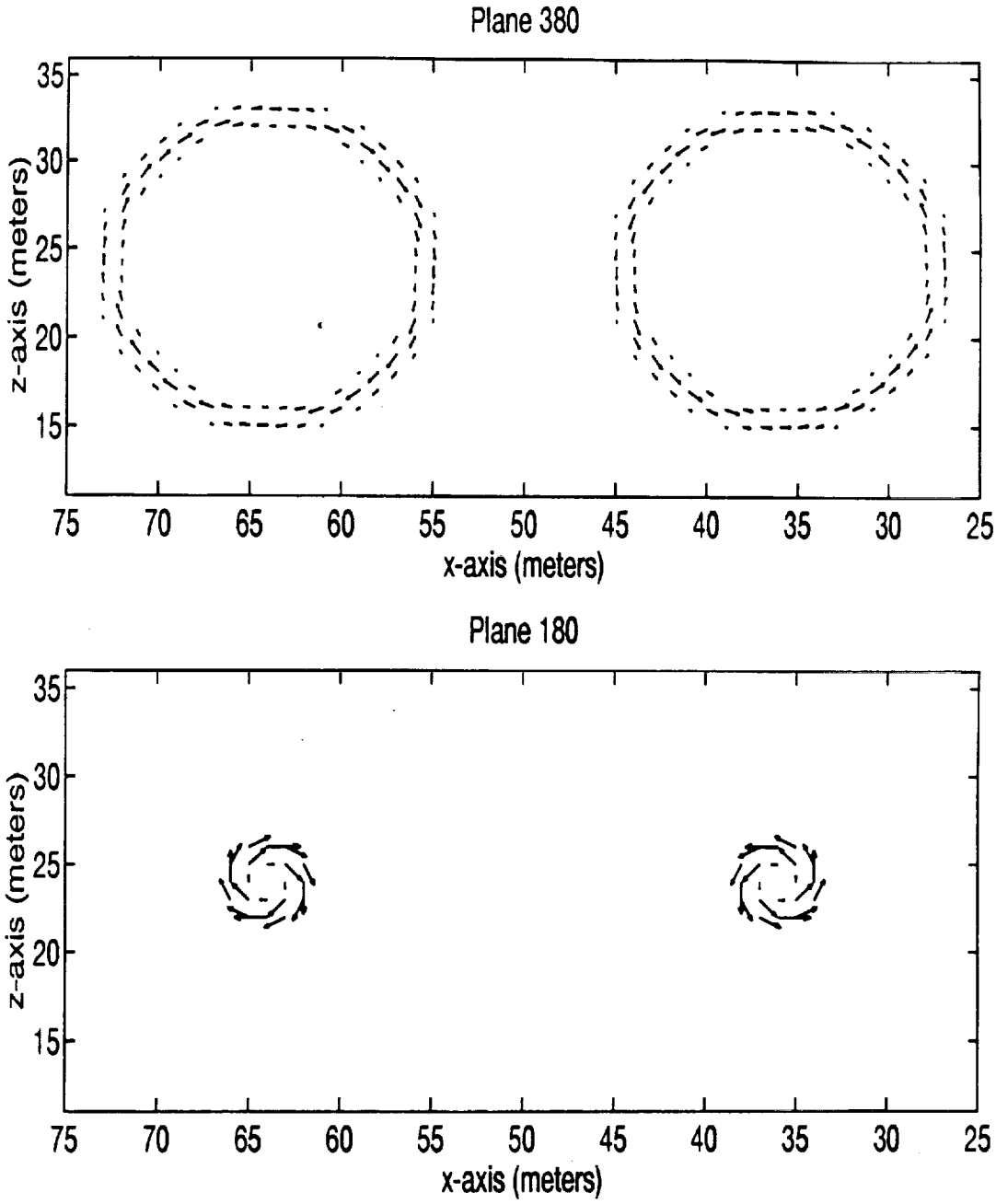

Figure 2.8 Actual YZ components of vortex rings.

2.3 Remote Sensor Placement

It is envisioned that a ground based remote sensor would be placed along the side of a runway at a height so that the sensor can look up into the vortex phenomenon, avoiding ground clutter pickup. Ground clutter can be severe in a radar return when the antenna beam is angled down into the earth. Analyses in this work primarily assume an ideal pencil beam antenna angled upwards by 4° with respect to the y-axis. Some view points were at vortex center height with a horizontal look direction. The view point typically was chosen to be at a height of 1 meter.

A secondary question is: Will the use of a single sensor be sufficient, or will multiple sensors enhance the "signature" detection capabilities. To test both cases, single view point positions were considered using a sequence of scanning elevation angles, from 13.5° to 40°, as illustrated in Figure 2.9. Multiple view point positions were analyzed using a fixed scan elevation angle, as shown in Figure 2.10.

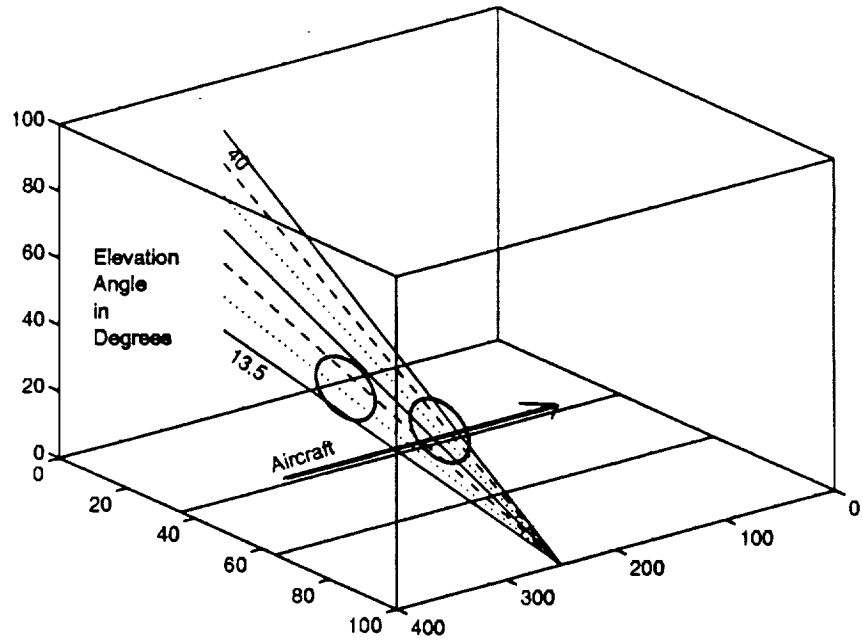

Figure 2.9 Single placement, multiple elevations.

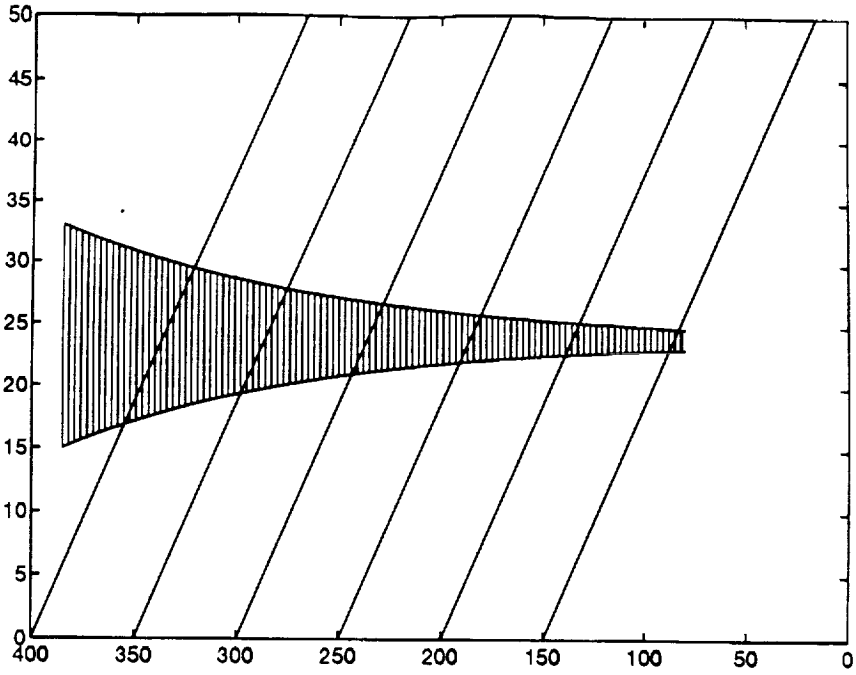

Figure 2.10 Multiple positions, but with a fixed elevation.

2.4 Scanning Angle Ranges

One of the more important components of the analysis is the ability to adjust the LOS angle in both the x and y direction. The x-axis angle is called the *tilt* angle, where a positive *tilt* indicates the LOS plane angles upward in the aircraft's flight direction. The y-axis angle is called the *elevation* angle. The *elevation* angle can be adjusted from -45 to +45° to give the radar the ability to sweep up or down across the runway. The test cases were restricted to an elevation of 0 to +45°. The *tilt* angle range includes -76 to +76° allowing horizontal to near vertical scans through the expanding wake vortex event. The tangent of the *elevation* angle is limited to a maximum of 1 (45°) while the tangent of the *tilt* angle is limited in magnitude to 4 (75.9°). Most of the experiments used either an *elevation* of zero with a positive *tilt* angle, or an *elevation* that passed through the aircraft's flight path with a *tilt* of zero. A linear interpolation scheme is used to determine the LOS windspeed vectors. Once the view point is established, for each x,y pair through the volume, the z position of

the LOS plane is calculated by

$$z = z_{reference} + tan(tilt) * (x_{reference} - x) + tan(elevation) * (y_{reference} - y).$$

Since the z position usually passes between two cell centers, the cell vectors are interpolated linearly between each of the two neighboring cells in the z-direction. These vectors are then projected onto the LOS for the simulation.

2.5 Dynamic Imaging Attempts

This model was developed primarily to represent a still image "snapshot" of a developed wake vortex so that a detectable "signature" could be found. Additionally, by using a series of incremental sensor placements, an evolution of the vortex signature might be attempted. Placement of the sensor at an initial view point, say x=150 meters, and then simulating the LOS image, would represent an initial time. Moving the sensor to larger x values (200, 250, 300, 350, and 400) and then performing additional simulations would effectively produce a set of time delayed images that mimic simulations from a fixed reference point onto a truly dynamic vortex. The author feels that this information will be valuable in determining the best LOS plane in which to detect the vortex event. Section 3.3 describes the results of this effort.

CHAPTER 3
RESULTS

The results presented in this chapter deal with two important questions concerning detection and tracking of the wake vortex phenomenon near an airport landing site. First, if technology enables design of a radar or lidar remote sensor that has the high-resolution (1-4meters) capabilities, would a detectable range Doppler "signature" of the wake vortex event be evident, and at what range resolution does this image become undetectable? Secondly, where and at what angle would the sensor detect a reliable image, i.e., how should a ground-based sensor be positioned and what scan strategies would be most advantageous? An explanation of the interest in multiple sensors is also presented.

3.1 Simulation Strategies

Four different approaches at scanning the search volume were taken, using combinations of the *tilt* and *elevation* angles. During the simulations, many volumes were created both with and without prevailing winds. There appeared to be no adverse affects on the clarity of the returns when a head or tail or side wind was present. Before the results are examined in detail, however, an example output is provided to aid in understanding the line-of-sight (LOS) evaluation program. Figure 3.1 shows an output of the LOS program. The "flight set" listed in the title refers to the requested simulation model from which the windfield components were extracted. This particular output used the set in "data" which was a calm air, 1 meter resolution model with wake vortex cell magnitudes up to 18 knots. The reference point is an arbitrary sensor location provided for the LOS evaluation. Pictured on this plot, the reference point is at (300,101,22). The image is a contour plot based on preset values, denoted in the lower right corner of the figure. This smaller window shows the possible windspeed

contour values used by the simulation, and the actual windspeed values (highlighted by asterisks) represented in the figure. The labeling of the contours is done as part of the program, but the user of the software must manually pick the points to to be included. Any output images from which figures in this chapter were extracted can be found in Appendix B.

The first results included no *elevation* or *tilt* angle with the view point placed near the aircraft height. This strategy is not intended to indicate a practical placement of the sensor, but as a test point to establish the validity of the model. Ground clutter is not considered here, but it is recognized that some antenna *elevation* would likely be needed to eliminate any ground clutter in an actual radar return. This experiment gave returns that were readily checked by hand so that the model could be verified. Figure 3.2 shows contours of LOS windspeed in the horizontal plane at several heights just below the center of each vortex with the XY position of the view points fixed. There is no prevailing wind, and the cell resolution is at 1 meter. In each figure, the right vortex (with positive windspeeds) is presented, instead of both the right and left vortex. The height of the returns varies from 22 meters in (A), to 18 meters in (D). As the height decreases, the LOS plane encounters less and less of the vortex, as shown by Figure 3.3. This figure corresponds to Figure 3.2, indicating where the planes of intersection occur. The LOS contour magnitudes (listed under A-D in Figure 3.2) show an increase and then decrease in strength as the LOS intersection plane gets lower. The best image is (C) with a range that has windspeed gusts of up to 16 knots. From (A) to (C), the increase is due to the LOS plane encountering more of the edge magnitudes along the radial axis of the vortex. However, the reduction seen in (D) is because the edges being encountered have a weaker magnitude. As the vortex expands away from the aircraft, it also weakens in intensity. One conclusion drawn here is that there is an optimum distance from the vortex core for a scan plane as indicated by Figure 3.2(C). A problem exists because the diameter of the vortex

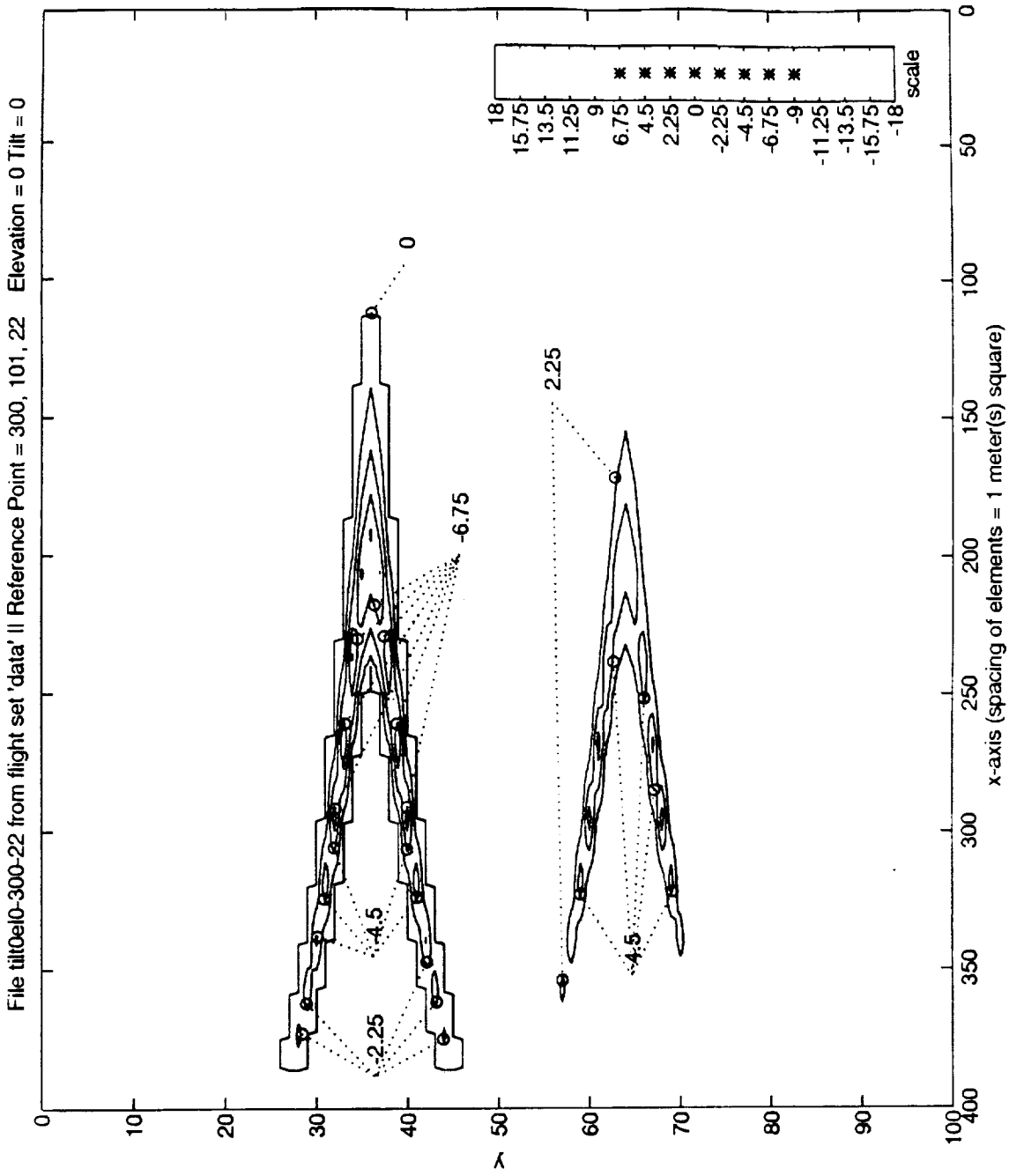

Figure 3.1 Example LOS output, using the specified simulation model "data".

depends on both the generating aircraft's wingspan, as well as the prevailing wind conditions, thus making it difficult to take advantage of this knowledge.

The second set of simulations involved a sensor view point position at a height of 1 meter, with a positive scan *elevation* angle so that the scan plane passed through the aircraft's entry path. This meant using the *elevation* angle only, since the flight path was assumed to be linear and parallel to the runway. Note that for a true flight path, a combination of the *elevation* and *tilt* angles could be easily calculated to maintain an alignment of the LOS plane with the flight path, since the flight path position is readily available. As seen in Figure 3.4, however, by passing through this angle, only positive windspeeds are encountered. This is due to the fact that the near vortex is encountered in the lower hemisphere where the wind direction is toward the sensor, while the far vortex intersects the plane in the upper hemisphere, again where the wind direction is toward the sensor, as illustrated by Figure 3.5. From the standpoint of detection, a vortex signature with the largest range of possible windspeeds will probably be best. This can be accomplished by adjusting the *elevation* angle to a fixed angle either below or above the flight path, so that both headwinds and tailwinds are encountered in the LOS plane to produce a wider windspeed magnitude range.

The next step was to lower the *elevation* angle to a fixed point below the flight path. A reduction by 5° resulted in the LOS plane passing just above the center of one vortex, as seen in Figures 3.6 and 3.7. The results show a much wider variation of windspeed components than for the situation in Figures 3.4 and 3.5. However, vortex dimensions vary and for a smaller vortex, a drop of 5° could position the LOS plane well below the center of the vortex, as shown in Figures 3.8 and 3.9. The range Doppler signature in Figure 3.8 is much less distinguishable. Similar results can be verified by raising the *elevation* angle above the flight path. From these results, it appears the scan elevation is significant in determining the vortex signature, but it may be difficult to rely on being able to predetermine the optimum scan angle in a given situation.

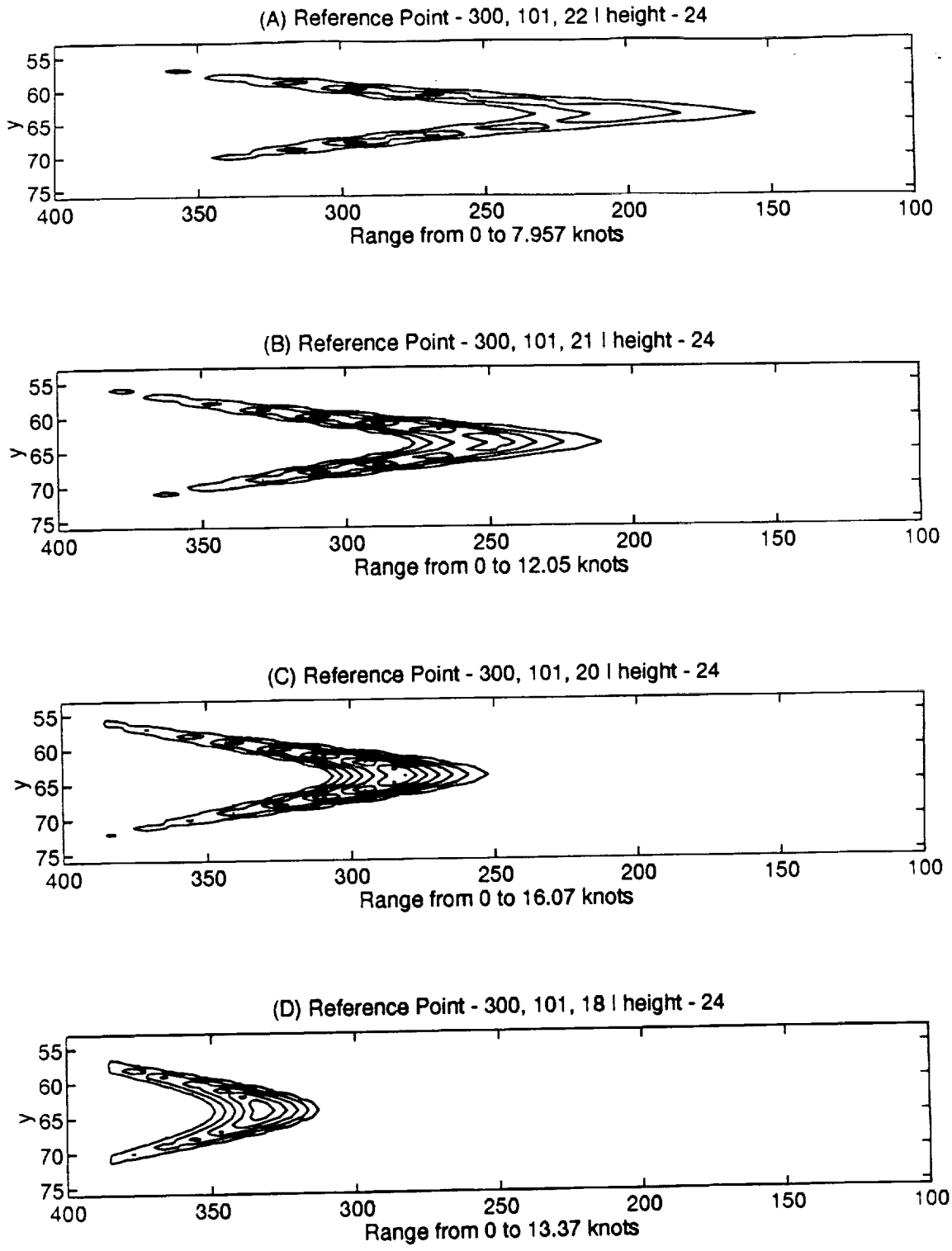

Figure 3.2 Horizontal view of vortex center.

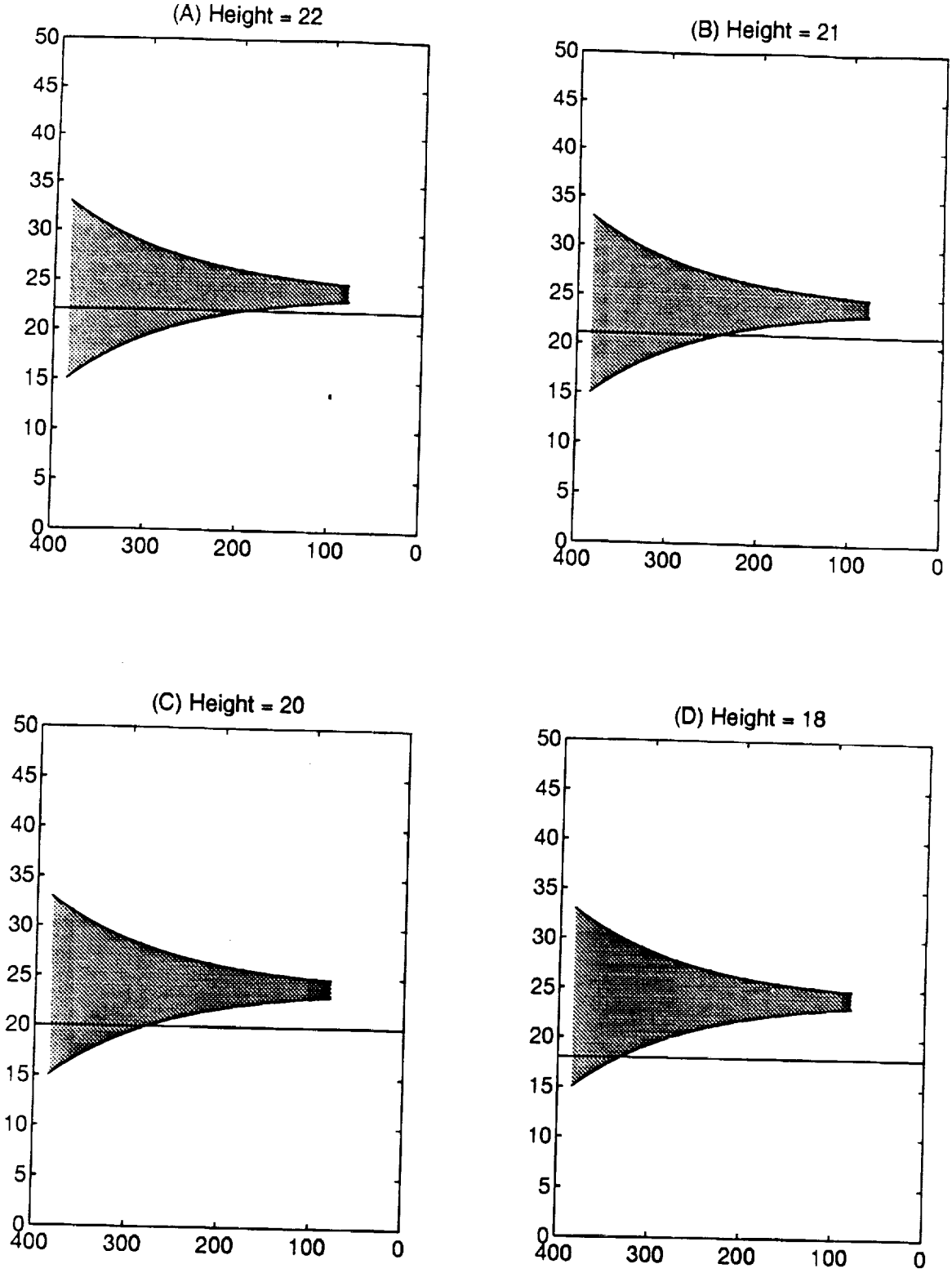

Figure 3.3 Plane through which LOS is calculated for previous figure.

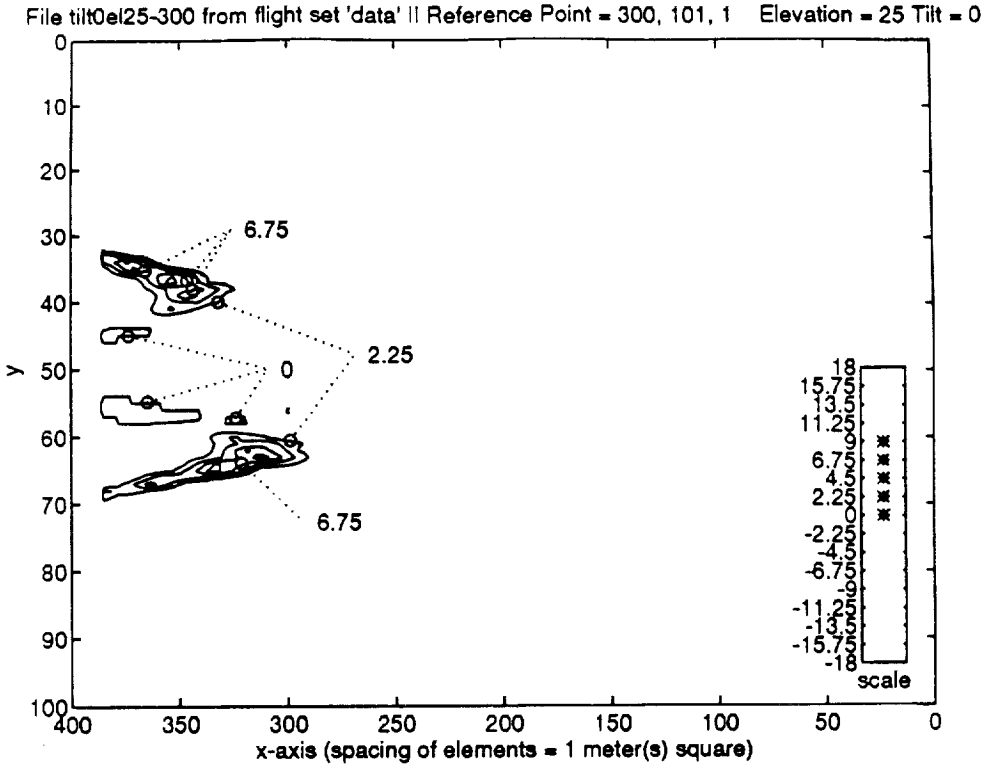

Figure 3.4 Results of passing LOS through the flight path.

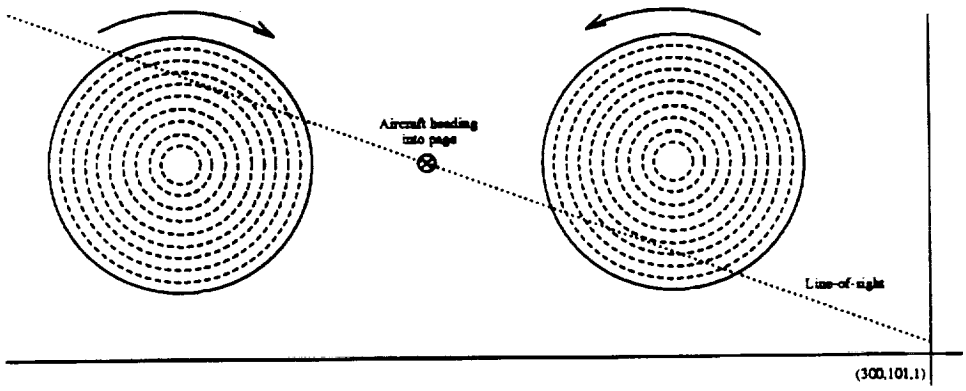

Figure 3.5 Two-D view of LOS intersection through flight path.

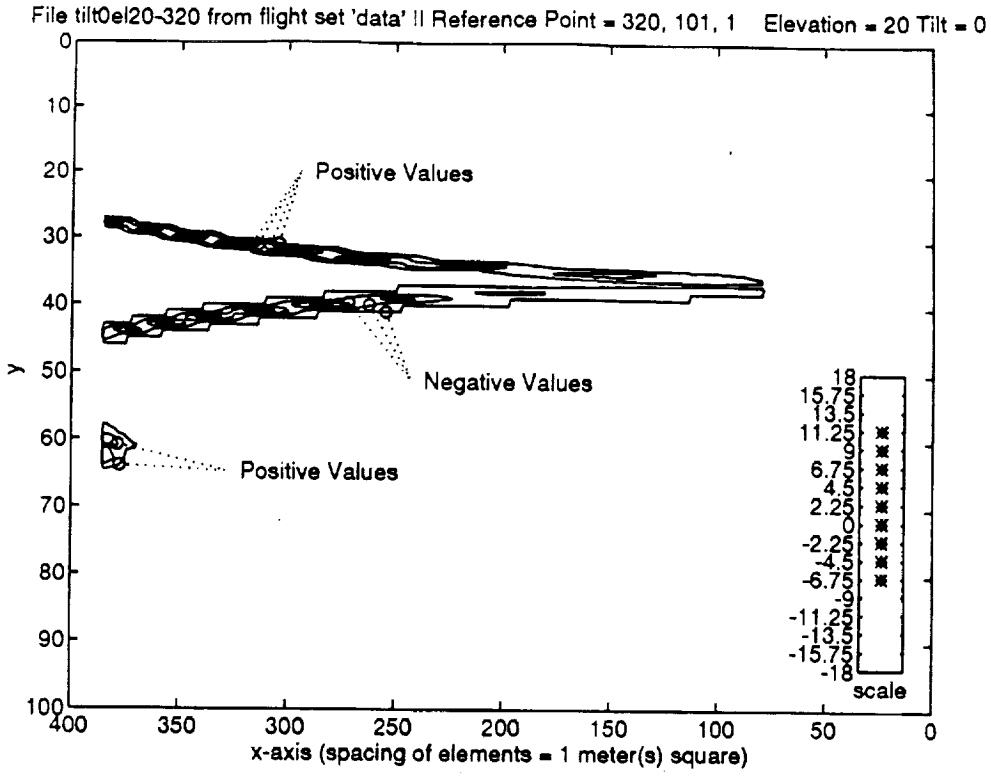

Figure 3.6 Results of passing LOS near vortex center.

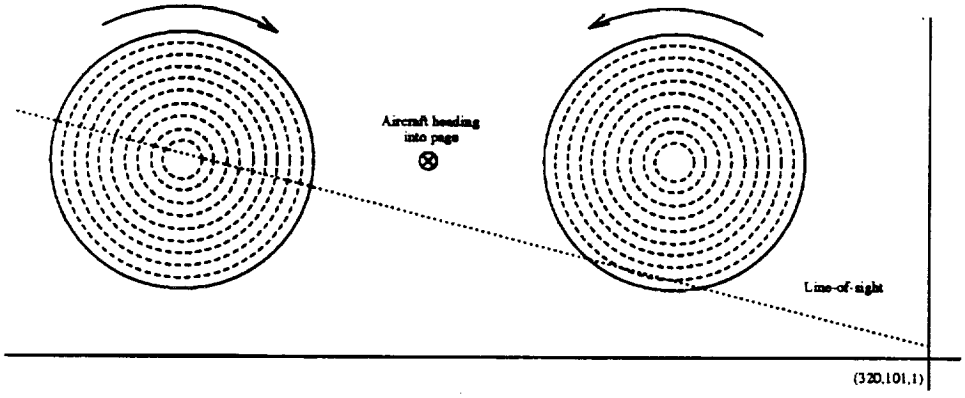

Figure 3.7 Two-D view of LOS intersection near vortex center.

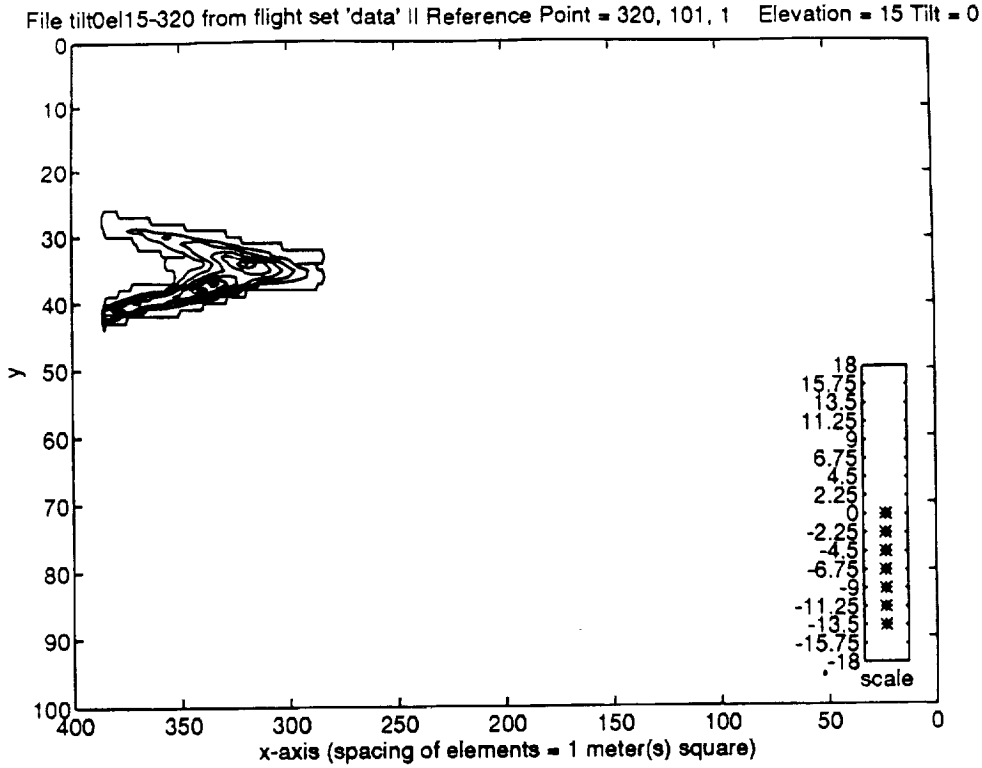

Figure 3.8 More realistic results of lowering LOS plane.

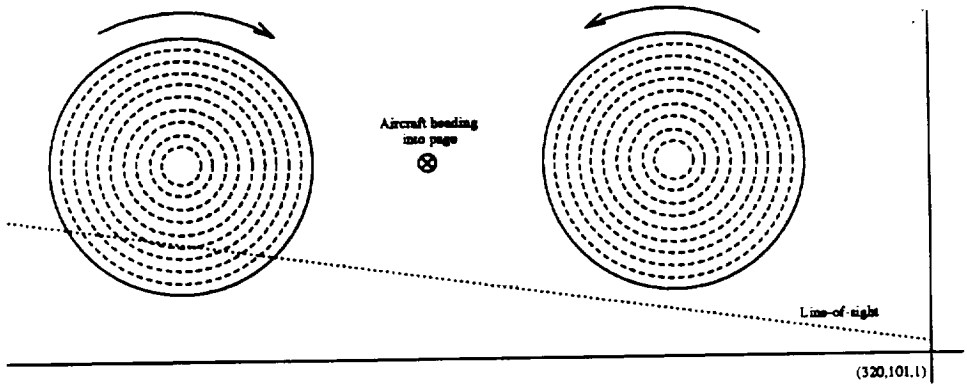

Figure 3.9 Two-D view of a LOS plane with a reduced *elevation* angle.

The third simulation involved variation of the *tilt* angle only. The results of the first two simulations suggested that to obtain the widest windspeed magnitudes variation, a LOS angle intersecting both hemispheres of a vortex would provide such a range. In addition, by selecting a fixed *tilt* angle, the size and entry angle of the aircraft generating a vortex would become relatively unimportant variables. Figure 3.10 and Figure 3.11 show the results of the LOS plane at a *tilt* angle of 15° relative to the x-axis, and positioned at x=270 and x=400, respectively. Note that the data set is "data-prevailing" which happened to be a data set with a non-zero prevailing wind condition. Figure 3.12 shows the intersection of the LOS plane and the two sensor placements viewed from the side. The straight lines seen in Figures 3.10 and 3.11 are evidence of the headwinds present in the windfield volume. Both the positive and negative hemispheres are present, but the intersection of cells that contain the vortex has been reduced. Even at a larger vortex core (x=400), the return would need a fine resolution in order to detect the positive and negative windspeeds.

The final simulation considered varying both *tilt* and *elevation* angles to achieve the most distinctive signature. Unfortunately, no significant increase in signature uniqueness was discovered. Section 3.4 illustrates some examples of combination angles. Using a complex angle only marginally increased the windspeed magnitude range captured within the LOS intersection plane. These increases, however, were heavily dependent on the size and position of the vortex, similar to the results found by just using the *elevation* angle.

3.2 Signature Development

The flight simulations and subsequent LOS computation using various combinations of angles, prevailing winds, and sensor placements yielded two similar types of signatures, each having a wide variation of windspeed magnitude. The major difference was in the shape of the signatures and the location of the peaks of positive and negative windfield components. Figure 3.13 shows the signature of choice. Taken

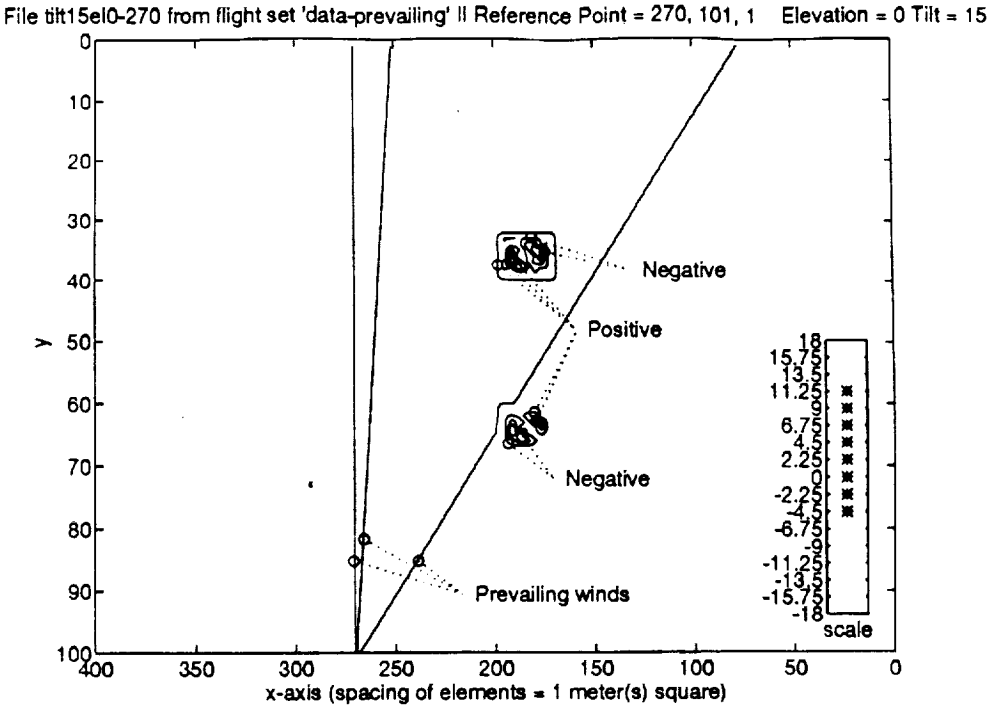

Figure 3.10 LOS plane tilted into vortex rings radially.

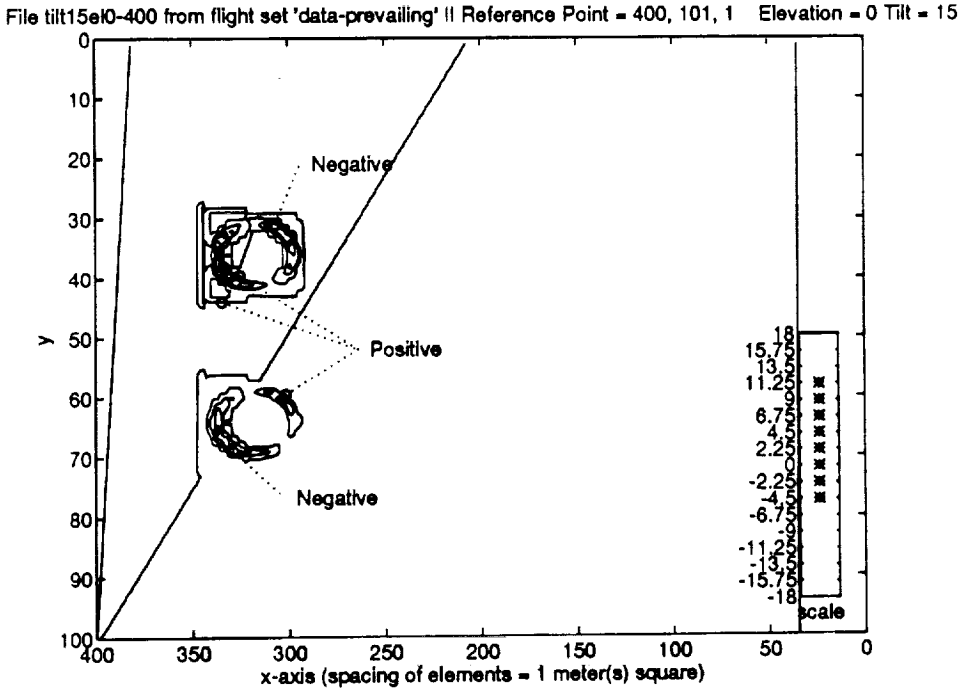

Figure 3.11 Tilted LOS at a later x-axis reference point.

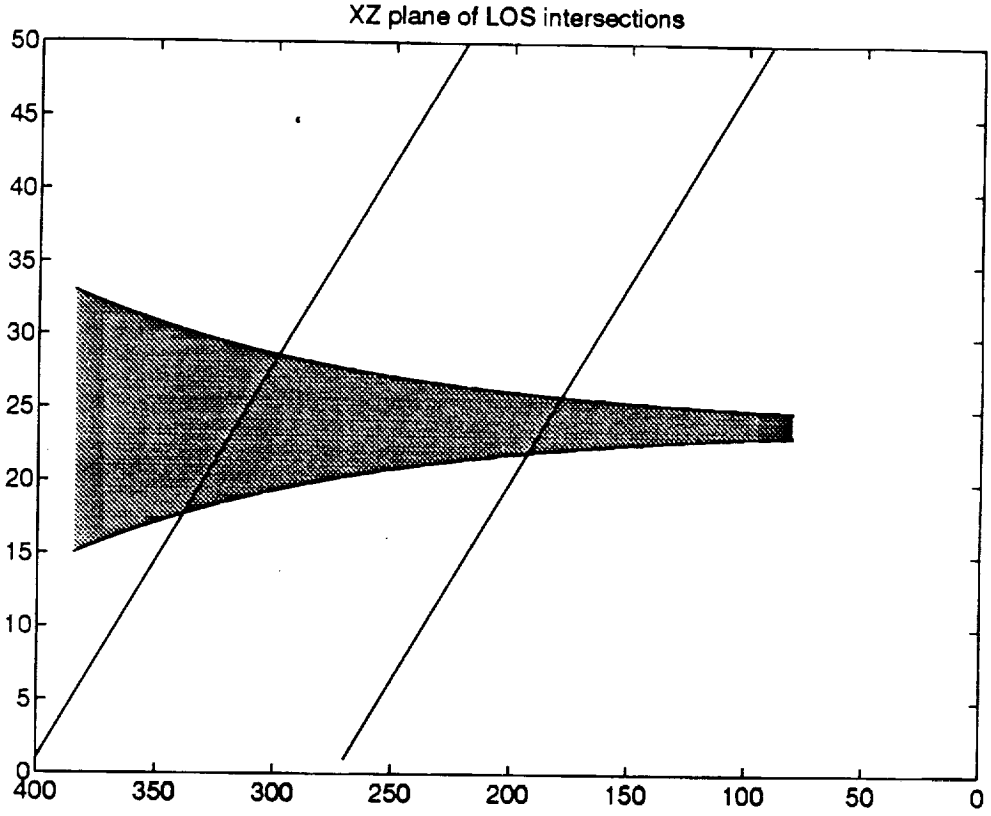

Figure 3.12 Side view of simulation using *tilt* angle only.

from Figure 3.11, this signature is circular in nature and has a positive and negative peak in a small, well defined area. The positive peaks are on the left half of the image, while the negative values are on the right. A three dimensional look at these peaks is illustrated in Figure 3.14. The placement of the sensor is not critical, and as the vortex grows radially, the returns increase in size. The decrease in magnitude of the windfield components only slightly affects the clarity of the return.

The type signature presented in Figures 3.4–3.8 depends more heavily on information about the aircraft's position, the prevailing wind conditions, and the size and location of the wake vortex itself. The advantage to this signature is that it encompasses a much larger area within the LOS plane, making it easier to track over time, and enabling signature recognition with a coarser cell resolution. Figure 3.15 shows this type signature pattern. It is no longer circular, but v-shaped, and the peaks are staggered in pockets of local maximums and minimums, which is also illustrated by Figure 3.16.

3.3 Dynamic Expansion

The placing of the sensor along incremental x-axis positions would effectively convey a time sequential set of images, as if the sensor had been fixed at a single point yielding staggered LOS planes as time passed. Figure 3.17 shows the evolution of the vortex event by moving the reference point from 200, to 270, to 350 and to 400, as shown in (A), (C), (E), and (G). The diagonal lines in the lower right corners are the result of the prevailing windspeed used in the simulation, and can be ignored. As noted in each image, the range is widely distributed but tightly centered. Figure 3.18 also demonstrates a dynamic capability from the second type of signature.

It appears that the ability to detect these phenomenon will be aided by multiple LOS scans as the aircraft passes, so that any developing vortex events can not only be detected, but tracked as time passes so that the next aircraft can avoid the event completely.

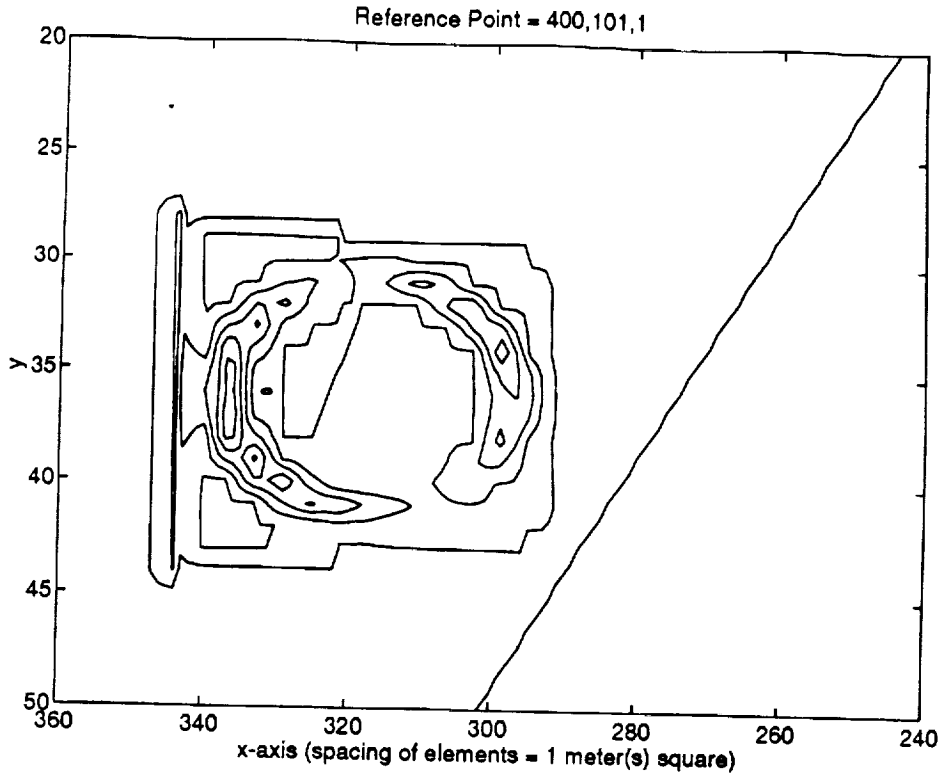

Figure 3.13 Signature type 1 primarily from a *tilt* angle.

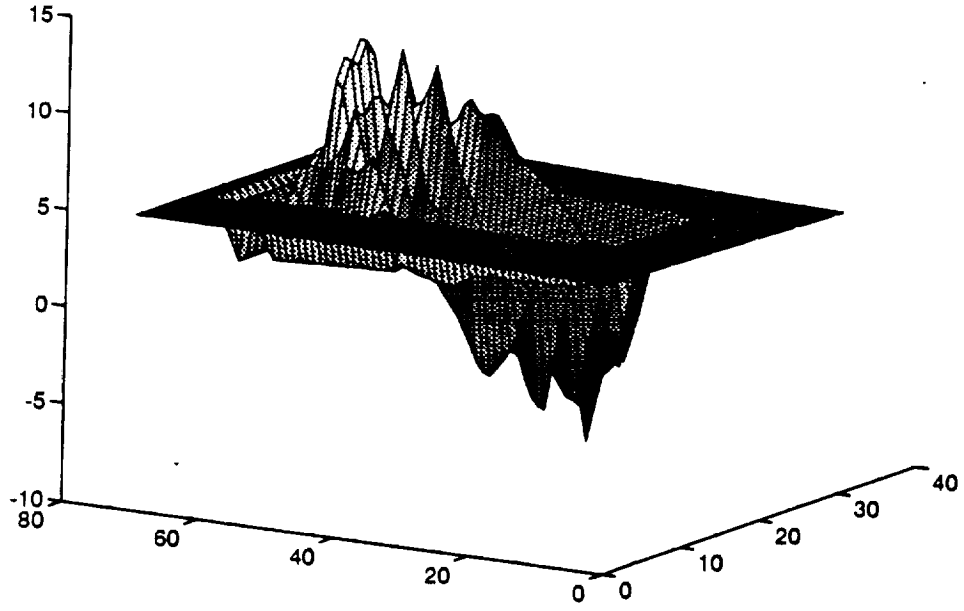

Figure 3.14 Three dimensional view of signature peaks.

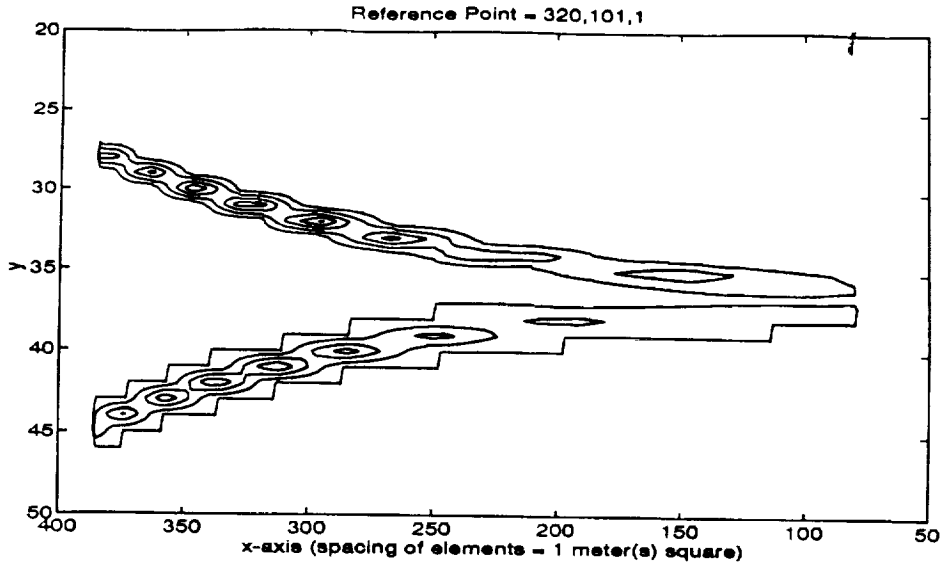

Figure 3.15 Signature type 2 primarily from an *elevation* angle.

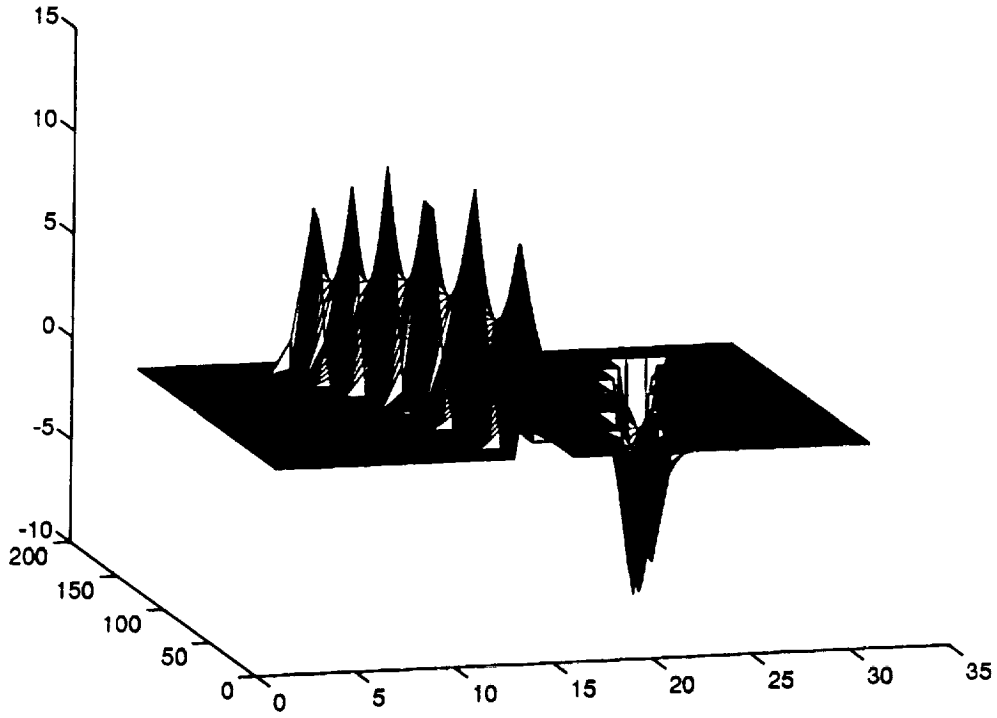

Figure 3.16 Three dimensional view of signature peaks.

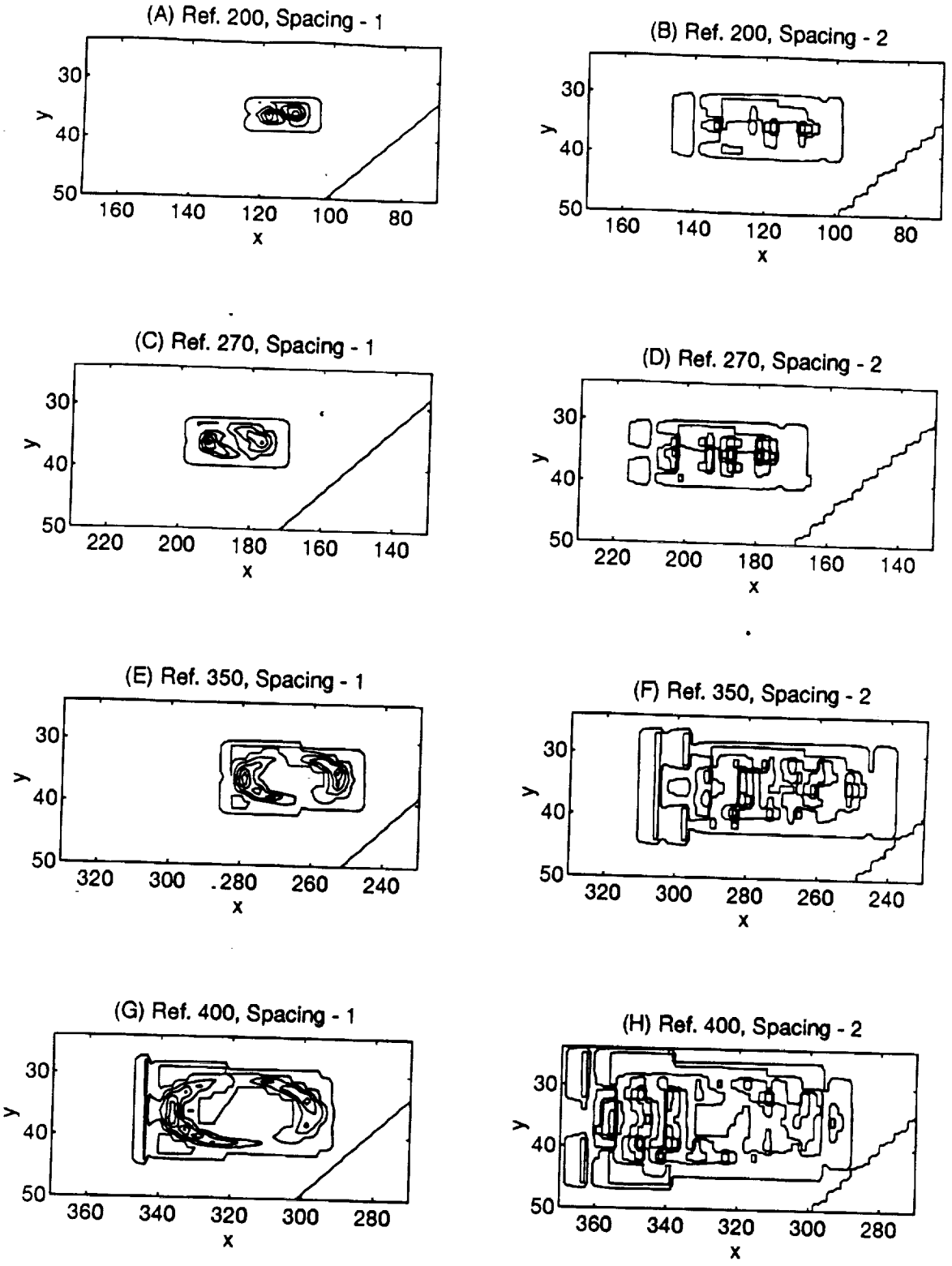

Figure 3.17 Signature development.

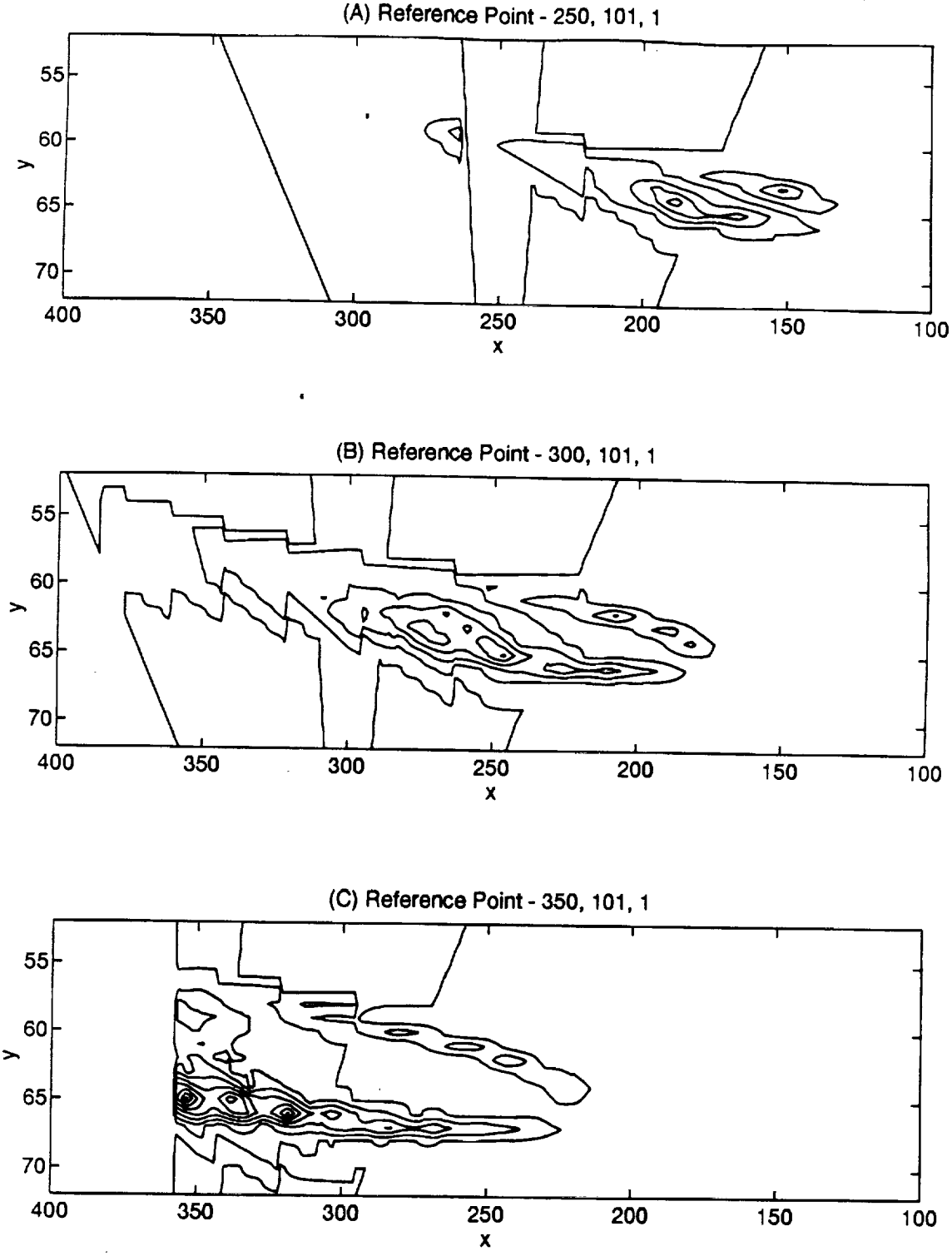

Figure 3.18 Signature of vortex using *tilt* of 4° and *elevation* of 24.27°, with 1m resolution.

3.4 Scale Effects on Signature Clarity

As described in section 2.2, this work considers cell resolution varying from 1 to 4 meters. Since the vortex spatial distortions often occupy a span of less than 10 meters in diameter, the smaller resolution allows for an improved clarity. Figure 3.17 shows type 1 signatures for both 1 and 2 meter cell widths. Figure 3.18 shows some type 2 signatures with a resolution of 1 meter. These images are for a combination *tilt* and *elevation* angle and do not encompass the wide range demonstrated by a type 1 signature. Figure 3.19 shows the same angle, but with a resolution increased to 2 meters. Finally, Figure 3.20 looks at the vortex using a 4 meter cell. The clarity of the LOS information is greatly compromised at even a 4 meter resolution, although with signal processing, meaningful information might still be obtainable.

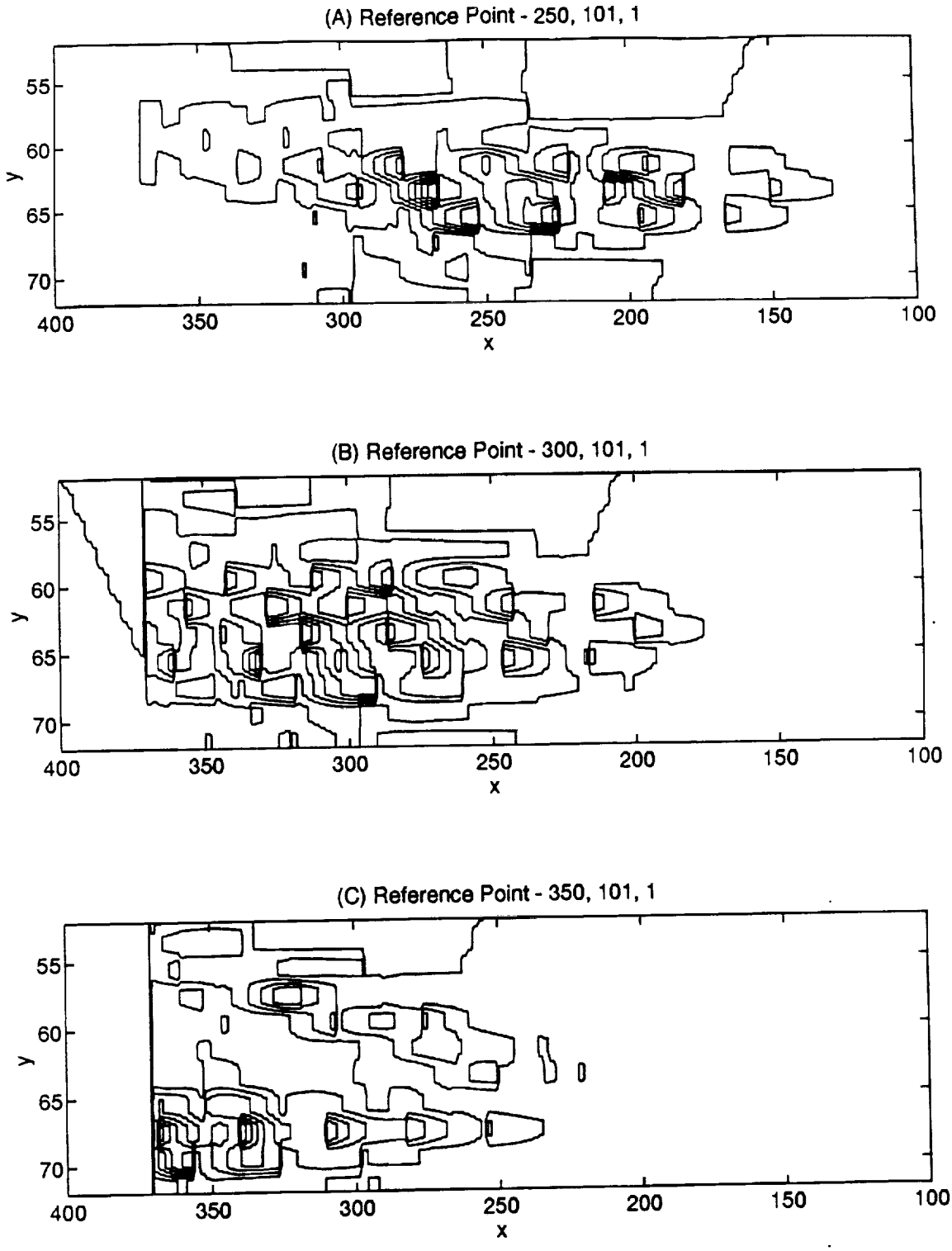

Figure 3.19 Signature of vortex using *tilt* of 4° and *elevation* of 24.27°, with 2m resolution.

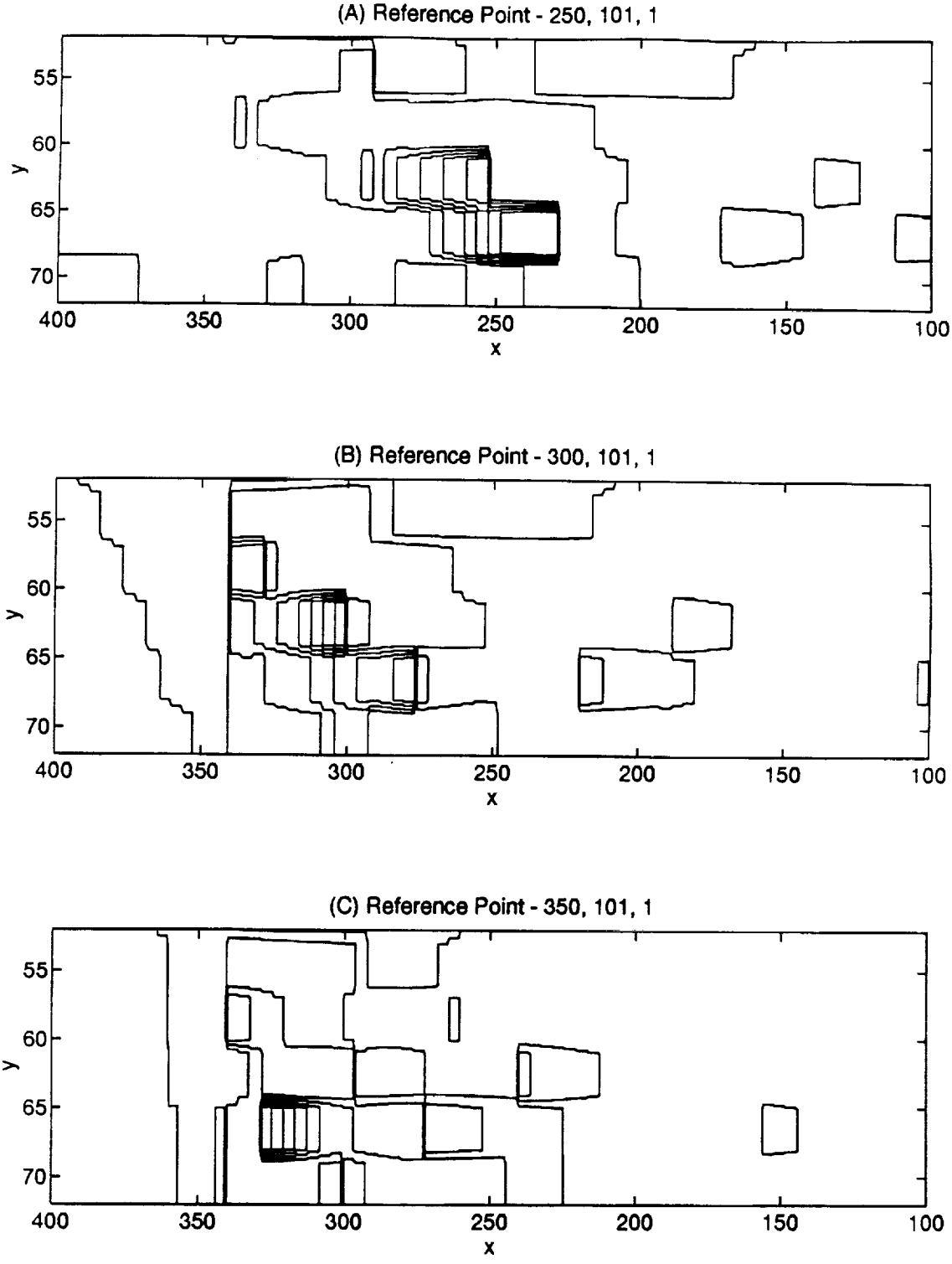

Figure 3.20 Signature of vortex using *tilt* of 4° and *elevation* of 24.27°, with 4m resolution.

CHAPTER 4
CONCLUSIONS

Reliable detection of the wake vortex phenomenon on final approach is a major technical problem, the solution to which can have a major impact on terminal area productivity. Safety concerns mandate separation minimums which are representative of a worst case scenario, generally when a small aircraft follows a large aircraft in final approach. On the other hand, if separations can be determined on the basis of actual hazards, there is potential for increasing terminal area productivity. The application of existing technology and the development of new technologies needed to detect and track the wake vortex is a major concern within the air traffic control community. This thesis addresses the application of a range-Doppler remote sensor by investigating the signature characteristics of the wake vortex.

Other works [9] have explored the possibility of detection of these events by measuring the temperature gradient between the low pressure core of a vortex relative to the ambient air temperature, with unclear results. Past works have primarily focused on using existing technology to solve the problem. While it is not the intent of the author to suggest that current technology is necessarily inadequate, the work discussed here depends upon technology advancement. It suggests a much finer spatial resolution system than is currently available with conventional search and weather radar or lidar systems. If technology is advanced to the point that very high range and Doppler resolution becomes available with an active pre-located remote sensor, two specific questions can be addressed. First, can the wake vortex return present a detectable signature? Second, is there a range-Doppler characteristic which is unique to this event which can be reliably identified?

This presentation has not considered the reflectivity of the turbulent air. Certainly this will be a major problem. Reflectivity with radar or lidar will depend upon

the presence of an aerosol in the vortex windfield, the type of aerosol, particle size, and many other factors. In any event, it is anticipated that the reflectivities will be very low. In conventional radar, range resolution is increased by reducing the pulse length, which generally means a lower duty factor and lower return power. Reflectivity of the target is critical and with systems operated at low altitude, the ground clutter can be expected to be significant. Other factors that are beyond the scope of this work are the effects of a realistic antenna beam pattern and the side lobe returns. These issues have not been addressed here.

The intent of the material presented here is to help gauge the need to explore higher resolution equipment, specifically for the task of wake vortex detection. NASA LaRC is currently working on a lidar system that is inherently within an order of magnitude of the resolution assumed in this study. There is also an effort to determine the feasibility of radar. Another related topic involves the location of the remote sensor and the scanning strategies that work best. The windfield model used here is admittedly simple and has been developed to demonstrate the analysis approach as well as to attempt to draw some general conclusions. This analysis can be applied to any vortex windfield model.

Based on analysis presented in this study, it is concluded that unless spatial resolution can be refined to within 5 meters, it is doubtful that a range Doppler signature identification can be reliable. However, for this resolution, some conclusions can be made. Horizontal scans are very much dependent on how the vortex is penetrated and would likely need both horizontal and vertical scanning. An alternative would be to use a tilted scan strategy. Looking into the the core of the vortex appears to give better results than a transverse, cross-runway look.

Future work could focus on the model itself, to generate a more realistic wake vortex event within the windfield. Inclusion of the x-axis windfield components, for example, could yield results with a greater magnitude range. Whatever the vortex model used, the LOS analysis software will perform as it does currently. Other areas

to consider could include incorporating the antenna beam pattern into the LOS software, or developing reflectivity analysis that would make fewer assumptions about the aerosol content and dispersion in the volume. Innovative signal processing strategies to provide enhanced range resolution while maintaining high duty factors with a pulsed Doppler sensor will undoubtedly be very important in detecting these low reflectivity events.

APPENDICES

Appendix A

Model Parameters and Source Code

The first listing is the parameter file that one edits prior to building a sampled windfield model containing a vortex pair. The programs were written in MATLAB, a UNIX based mathematical software package.

```
% This is a script file that sets up the wake vortex parameters
% according to programmer specifications.
% All information is global, and always available to user.

% Cubic Information for the field of view (m)
% Y and Z must be square in dimension to allow program processing
  XMIN = 0;
  XMAX = 399;
  YMIN = 0;
  YMAX = 99;
  ZMIN = 0;
  ZMAX = 99;

% Spacing between elements in the xyz volume, or 1/(# blocks per m^2)
% A spacing of 1 would mean for a 4x4x4 meter block there were 64 arrow vectors
% A spacing of 2 would mean for a 4x4x4 meter block there were 8 arrow vectors
% A spacing of 4 would mean for a 4x4x4 meter block there was 1 arrow vector
  spacing = 1;

% The calculated values are normalized from 0 to 1 for the windspeed magnitudes.
% However the truth data is limited by the WSPDMAX value that
% indicates the airspeed range in knots (-WSPDMAX to WSPDMAX)
  WSPDMAX = 18;

% Prevailing wind speeds in each direction (units are in knots)
  prvx = 3;
  prvy = 4;
  prvz = 0.5;

% Maximum radius of the vortex (m)
  final_radius = 9;

% Distance from left and right of center of runway to the vortex center (m)
  w0 = 14;

% Height of vortex center above ground zero (m)
  h0 = 24;

% Limit on the range around the true circle that is acceptable
  limit = 1/1.1;
```

The next section contains the source code that generated the volume of windspeed components.

```
% WAKE1.M is a script file that builds a volume air flow over a runway that
%         contains a wake vortex pair.
% Load all constant values from file
  clear
  disp([' ';' ';' '])
  disp('*************************************************************************')
  disp('***                                                                   ***')
  disp('***   Wake vortex modelling program - Written by Bob Heil 3/94        ***')
  disp('***                                                                   ***')
  disp('*************************************************************************')
  disp('   Loading parameters and setting up cubic volume.')
  params  % Loads a script file that has the constant values in it

  space_adjust % Set up parameters based on spacing

% Vector for display of the x-axis rate of decay function
  r = zeros(xstop-x0+1,2);

  disp([' ';' '])
  disp('   The following parameters are set: (units are meters)')
  disp(['   Width of runway = ',int2str(run)])
  disp(['   Height from ground to center of vortex = ',int2str(hgt*spacing)])
  disp(['   Distance to the 1/r center of runway = ',int2str(wid*spacing)])
  disp(['   The decay = ',int2str(r0*spacing),' e^(-t/',num2str(rate),')'])
  disp(['   The prevailing wind is ',num2str(prvx),' by ',num2str(prvy),...
        ' by ',num2str(prvz),' (knots)'])
  disp(['   The scale factor is ',num2str(spacing),' meter(s) cubed'])
  disp(['   The vortex maximum windspeed is +/- ',num2str(WSPDMAX),' (knots)'])
  disp('  ')
  disp('   Strike any key to begin run  ')
  disp('  ')
  pause

% Turning the hold on so that the yz planes will accumulate on one plot
% hold on

% Will now do the evaluation of the data based on the x-axis
  for x = 1:xtotal
    disp(['Slicing thru ',int2str(x),' of ',int2str(xtotal)])
       eval(['x',int2str(x),' = prvx + zeros(ytotal,ztotal);'])
       eval(['y',int2str(x),' = prvy + zeros(ytotal,ztotal);'])
       eval(['z',int2str(x),' = prvz + zeros(ytotal,ztotal);'])
    % For each plane in the active vortex area:
       if ((x >= x0) & (x <= xstop))

      % Set up the values for the vortex model
      radius = r0*exp(-(xstop-x)/rate); % Current vortex radius
      r(xstop-x+1,1) = radius;          % r tracks the changing radius over x
      r(xstop-x+1,2) = x;               %   by radius and position
```

```
MAX = round(radius) + 1;          % MAX denotes the largest space needed
                                  %     to hold the wind vector info
% Determine the sub-grid of values for the windspeed array values
[Ypos,Zpos] = meshgrid(-MAX:1:MAX);

% The array 'position' has the location of the vortex.  The closer each
%     element is to 0.0, the stronger the magnitude of the windspeed
position = sqrt(Ypos.^2 + Zpos.^2) - radius;

% Take any Ypos = 0 and set to 1e-11 to prevent DIVIDE by ZERO WARNING
for i = 1:size(Ypos)
    if Ypos(1,i) == 0
       for j = 1:size(Ypos)
           Ypos(j,i) = 0.00000000001;
       end
    end
end

% The 'angle' array is used to calculate the direction of the windspeed
%     in the array 'position'
angle = atan(Zpos./Ypos);

% Now we find the true location of the sub-array within the entire
%     [YMIN YMAX ZMIN ZMAX] array of space
[Ypos,Zpos] = meshgrid(center-MAX-wid:1:center+MAX-wid,...
                       -MAX+hgt:1:MAX+hgt);
% Find the number of elements in the sub-array
total = size(position);
total = total(1); % = total(2) since square!


% Create the actual array values in each direction based on the
%        prevailing crosswind and the wake-vortex.
ymag = zeros(total,total);
zmag = ymag;

sliceRight % Set the right-sided plane vortex y & z magnitudes

% Load the right side of the vortex into the larger array
s =  [int2str(x),'(',int2str(Zpos(1,1)),':',...
      int2str(Zpos(1,1) + total - 1),',',int2str(Ypos(1,1)),':',...
      int2str(Ypos(1,1) + total - 1),') = '];
eval(['y',s,'ymag;'])
eval(['z',s,'zmag;'])

% Redo for the other side of the vortex.
[Ypos,Zpos] = meshgrid(center-MAX+wid:1:center+MAX+wid,...
                       -MAX+hgt:1:MAX+hgt);
sliceLeft % Set the left-sided plane vortex y & z magnitudes

% Load the right side of the vortex into the larger array
s =  [int2str(x),'(',int2str(Zpos(1,1)),':',...
      int2str(Zpos(1,1) + total - 1),',',int2str(Ypos(1,1)),':',...
      int2str(Ypos(1,1) + total - 1),') = '];
```

```
      eval(['y',s,'ymag;'])
      eval(['z',s,'zmag;'])

    end

    % Save the x, y, and z array to file frame(x) eg. 'save frame80 x80 y80 z80'
    eval(['save frame',int2str(x),' x',int2str(x),...
          ' y',int2str(x),' z',int2str(x)])

    % Clear the workspace of the x, y, and z array to make room for the next
    eval(['clear x',int2str(x),' y',int2str(x),' z',int2str(x)])
  end % End of the For on X

  % Save the variables used for this flight in this directory

  eval(['save flight WSPDMAX XMAX XMIN YMAX YMIN ZMAX ZMIN h0 prvx ',...
        'prvy prvz r run spacing w0 final_radius'])
```

The last section contains the code that generates and plots the LOS plane images based on the simulation model.

```
% LOS.M  is a script file that calculates los information from the wake1 program
% Set up the graphics figure
  figure(1)
  set(1,'Position',[4 -870 1010 780])
  clf

% Load all constant values from file
  clear
  disp([' ';' ';' '])
  disp('*************************************************************************')
  disp('***                                                                   ***')
  disp('***  Wake vortex evaluation program - Written by Bob Heil 4/94        ***')
  disp('***                                                                   ***')
  disp('*************************************************************************')
  disp('  ')
  oldpath = pwd;
  newpath = input('Enter the directory of flight data to use -> ','s');
  eval(['chdir ',newpath])
  load flight
  eval(['chdir ',oldpath])

% Requesting the storage name
  name = input('Save name for New or Old data -> ','s');

if (input('   N for NEW run, any other key for old run -> ','s') == 'N')
  space_adjust % Set up parameters based on spacing

  disp([' ';' '])
  disp('   The following parameters are set: (units are meters)')
  disp(['   Width of runway = ',int2str(run)])
  disp(['   Height from ground to center of vortex = ',int2str(hgt*spacing)])
  disp(['   Distance to the l/r center of runway = ',int2str(wid*spacing)])
```

```
disp(['   The decay = ',int2str(r0*spacing),' e^(-t/',num2str(rate),')'])
disp(['   The prevailing wind is ',num2str(prvx),' by ',num2str(prvy),...
      ' by ',num2str(prvz),' (knots)'])
disp(['   The scale factor is ',num2str(spacing),' meter(s) cubed'])
disp(['   The vortex maximum windspeed is +/- ',num2str(WSPDMAX),' (knots)'])
disp('  ')
disp('   Strike any key to begin run  ')
disp('  ')
pause

% Obtaining the reference point for the calculations of line of sight
  xreq = input('X-dir Reference Point -> ');
  yreq = input('Y-dir Reference Point -> ');
  zreq = input('Z-dir Reference Point -> ');
  refx = round(xreq/spacing);
  refy = round(yreq/spacing);
  refz = round(zreq/spacing);

% Similar information for the elevation angle and the tilt angle
  disp('  ')
  disp(['To pass through the flight path use an elevation angle of ',...
        num2str(atan(abs((refz-hgt)/(refy-center)))*180/pi),' degrees.'])
  el   = input('Elevation angle in y  -> ');
       % el is in degrees where positive number indicates rise in angle
  tilt = input('Tilt angle in x (- clockwise, + counter clockwise) -> ');
       % tilt is in degrees where positive value indicates counter clockwise
  radel = tan(el * pi / 180);
  radtilt = tan(tilt * pi / 180);

% Will now do the evaluation of the data based on the x-axis
    eval(['chdir ',newpath])
    LOS = zeros(xtotal,ytotal);
    for x = 1:xtotal
    disp(['Evaluating plane x = ',int2str(x),' of ',int2str(xtotal)])
      eval(['load frame',int2str(x)])
      for y = 1:ytotal
      % Determine the z position of the element corresponding to x and y
        zval = refz + radtilt*(refx - x) + radel*(refy - y);
        if (zval >= round(zval))
           ratio = 1 - (zval - round(zval));
        else
           ratio = round(zval) - zval;
        end
        z = floor(zval);
        if (z <= 0 | (z+spacing)>=ztotal)
           LOS(x,y) = 0;
        else
           delx = abs(x - refx);
           dely = abs(y - refy);
           delz = abs(z - refz);
           dist = sqrt(delx^2 + dely^2 + delz^2);
           s1 = [int2str(x),'(z,y)'];
           s2 = [int2str(x),'(z+spacing,y)'];
           eval(['Wx = x',s1,' * ratio + x',s2,' * (1-ratio);'])
```

```
            eval(['Wy = y',s1,' * ratio + y',s2,' * (1-ratio);'])
            eval(['Wz = z',s1,' * ratio + z',s2,' * (1-ratio);'])
            LOS(x,y) = (Wx*delx + Wy*dely + Wz*delz)/dist;
         end
       end % end For y
       eval(['clear x',int2str(x),' y',int2str(x),' z',int2str(x)])
     end % end For x
     true_spacing = spacing;
     if spacing > 1
        fixLOS;
        refx = xreq;
        refy = yreq;
        refz = zreq;
        spacing = 1;
        space_adjust
     end
     eval(['chdir ',oldpath])
     eval(['save ',name,' LOS el tilt refx refy refz true_spacing'])

   else
     eval(['load ',name])
     spacing = 1;
     space_adjust
   end %

   % Display the line of sight plane of interest
   orient landscape
   lnum = 8; %How many contour lines
   L =  -WSPDMAX:WSPDMAX/lnum:WSPDMAX;
   c = contour(LOS',L);
   axis([0 xtotal 0 ytotal])
   first = gca;
   set(gca,'xdir','reverse','ydir','reverse')
   xlabel(['x-axis (spacing of elements = ',int2str(true_spacing),...
           ' meter(s) square)'])
   ylabel('y')
   b = findstr(newpath,'/');b = b(size(b));b=b(2)+1;e = size(newpath);e=e(2);
   datadir = newpath(1,b:e);
   title(['File ',name,' from flight set ''',datadir,''',...
          ' || Reference Point = ',int2str(refx),', ',int2str(refy),', ',...
       int2str(refz),'    Elevation = ',num2str(el),' Tilt = ',num2str(tilt)])

   scaleplot = axes('position',[.839 .16 .04 .36]);
   cdim = size(c);
   loop = 1;
   i = 1;
   while loop < cdim(2)
      smag(i,1) = c(1,loop);
      smag(i,2) = c(2,loop);
      xspot(i) = .5;
      loop = loop + c(2,loop) + 1;
      i = i + 1;
   end
   plot(xspot,smag(:,1),'c*')
```

```
axis([0 1 min(L) max(L)])
set(scaleplot,'xtick',[],'ytick',L)
xlabel('scale')

if (input('  L for Labelling plot, any other key to quit -> ','s') == 'L')
  set(1,'currentaxes',first)
  smag
  hold on
  t = input(' How many points do you want to label? ');
  for loop = 1:t
    u = input([' How many points on label # ',int2str(loop),' ? ']);
    disp(' Starting in the vortex and moving to the right, use the mouse to')
    disp('  click on the points for lines to be drawn, with the last click')
    disp('  designating the point to place the magnitude label')
    i = ginput(u+1);
    for v = 1:u
       line([i(v,1) i(u+1,1)],[i(v,2) i(u+1,2)],'color','g','linestyle',':');
       plot(i(v,1),i(v,2),'go')
    end
    point = input(' Enter the value for this point -> ','s');
    text(i(u+1,1),i(u+1,2),['  ',point])
  end
  hold off
end
```

Appendix B

Range-Doppler Wake Vortex Signatures

What follows is a set of line-of-sight (LOS) range Doppler images that depict various signature types. Different sensor placements and/or scanning strategies are included in these figures. The title of each image contains five pieces of information about the figure presented:

1. The file name is specified and in a shorthand method, provides the *tilt* and *elevation* angles used and the x-direction point of the sensor. For example: "tilt4el25-320" is an image positioned at (320,101,1) with a 4° *tilt* angle and a 25° *elevation* angle.
2. The flight set indicates what simulation model was used to generate the LOS image.
   - data - Prevailing wind (0,0,0)knots, *spacing* = 1*m*
   - data2 - Prevailing wind (0,0,0)knots, *spacing* = 2*m*
   - data4- Prevailing wind (0,0,0)knots, *spacing* = 4*m*
   - data-prevailing - Prevailing wind (3,4,0.5)knots, *spacing* = 1*m*
   - data2-prevailing - Prevailing wind (3,4,0.5)knots, *spacing* = 2*m*
   - data4-prevailing - Prevailing wind (3,4,0.5)knots, *spacing* = 4*m*
3. The reference point indicates the (x, y, z) position of the sensor.
4. The *elevation* angle defines the angle along the y-axis in the xy plane.
5. The *tilt* angle defines the angle along the x-axis in the xy plane.

The spacing of elements (denoted under each image) indicates the cell resolution for the model that was used in this image. The spacing ranges from 1m to 4m. The smaller window, in the lower right corner, shows the Doppler velocity range that the model covers, and depicts with an asterisk the ranges present in each image. The position of the aircraft is (80,50,24) and the runway is in the -x direction between y=36 and y=64 at z=0.

The first four images are of a horizontal plane that intersects the vortex transversely at decreasing heights. The next eight images are angled into the defined volume using only a tilt angle. The last 9 images utilize both the tilt and the elevation angles to form a hybrid signature that maintains wide magnitude ranges, but depends less heavily on the physical situation surrounding the vortex.

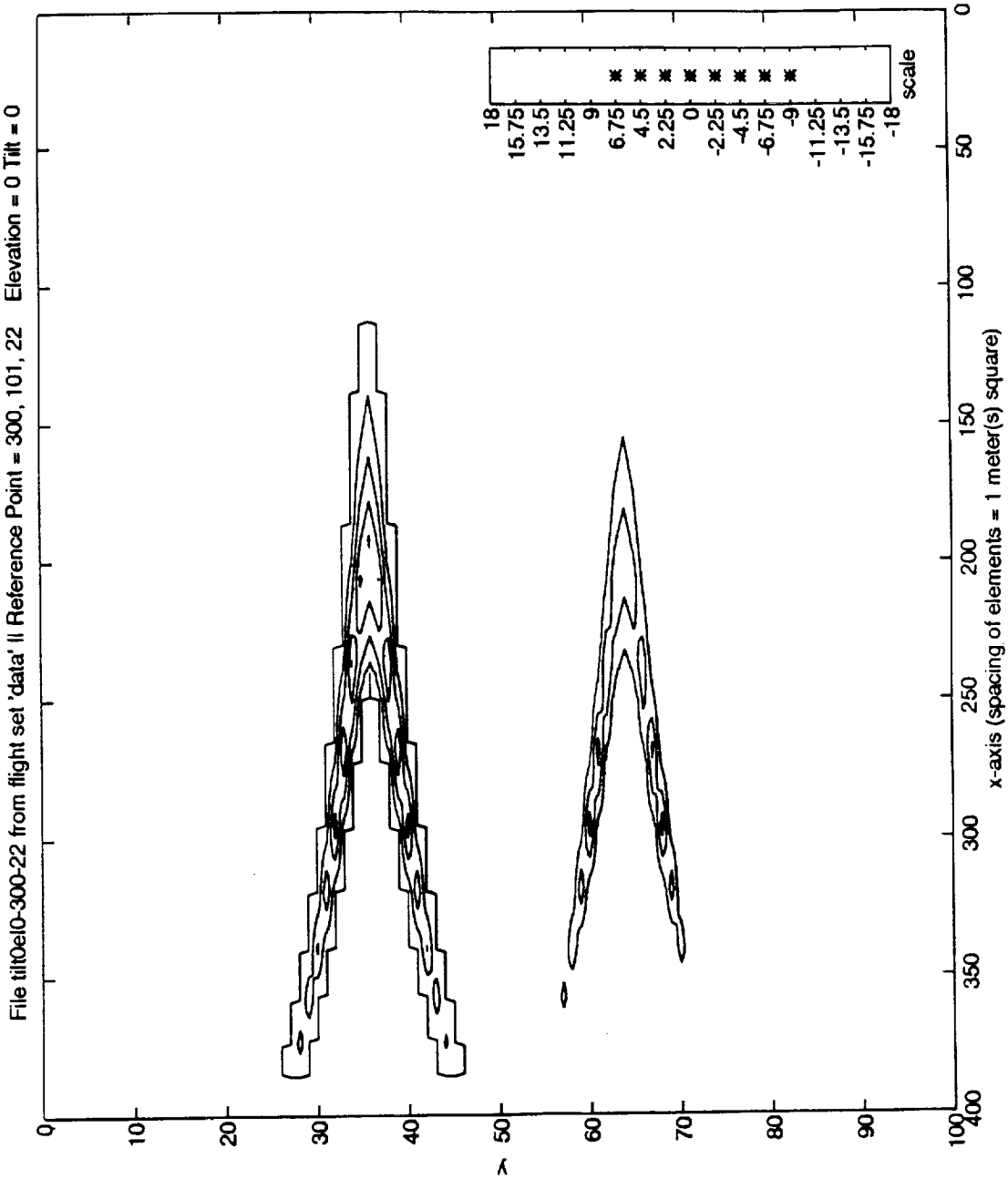
File tilt0el0-300-22 from flight set 'data' II Reference Point = 300, 101, 22 Elevation = 0 Tilt = 0
scale
18
15.75
13.5
11.25
9
6.75
4.5
2.25
0
-2.25
-4.5
-6.75
-9
-11.25
-13.5
-15.75
-18
x-axis (spacing of elements = 1 meter(s) square)
y
0
10
20
30
40
50
60
70
80
90
100
400
350
300
250
200
150
100
50
0

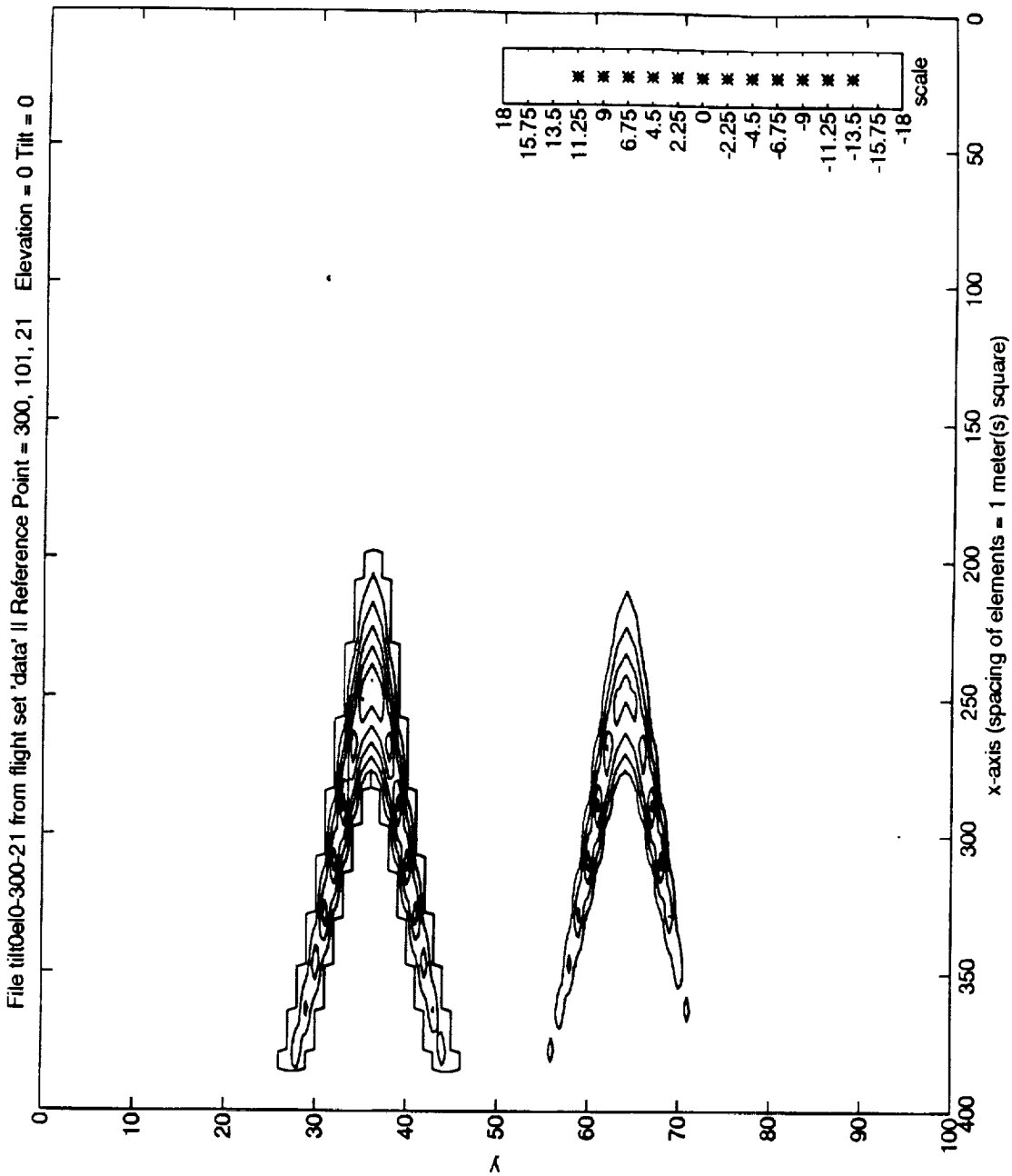
File tilt0el0-300-21 from flight set 'data' ll Reference Point = 300, 101, 21 Elevation = 0 Tilt = 0
18
15.75
13.5
11.25
9
6.75
4.5
2.25
0
-2.25
-4.5
-6.75
-9
-11.25
-13.5
-15.75
-18
scale
y
x-axis (spacing of elements = 1 meter(s) square)

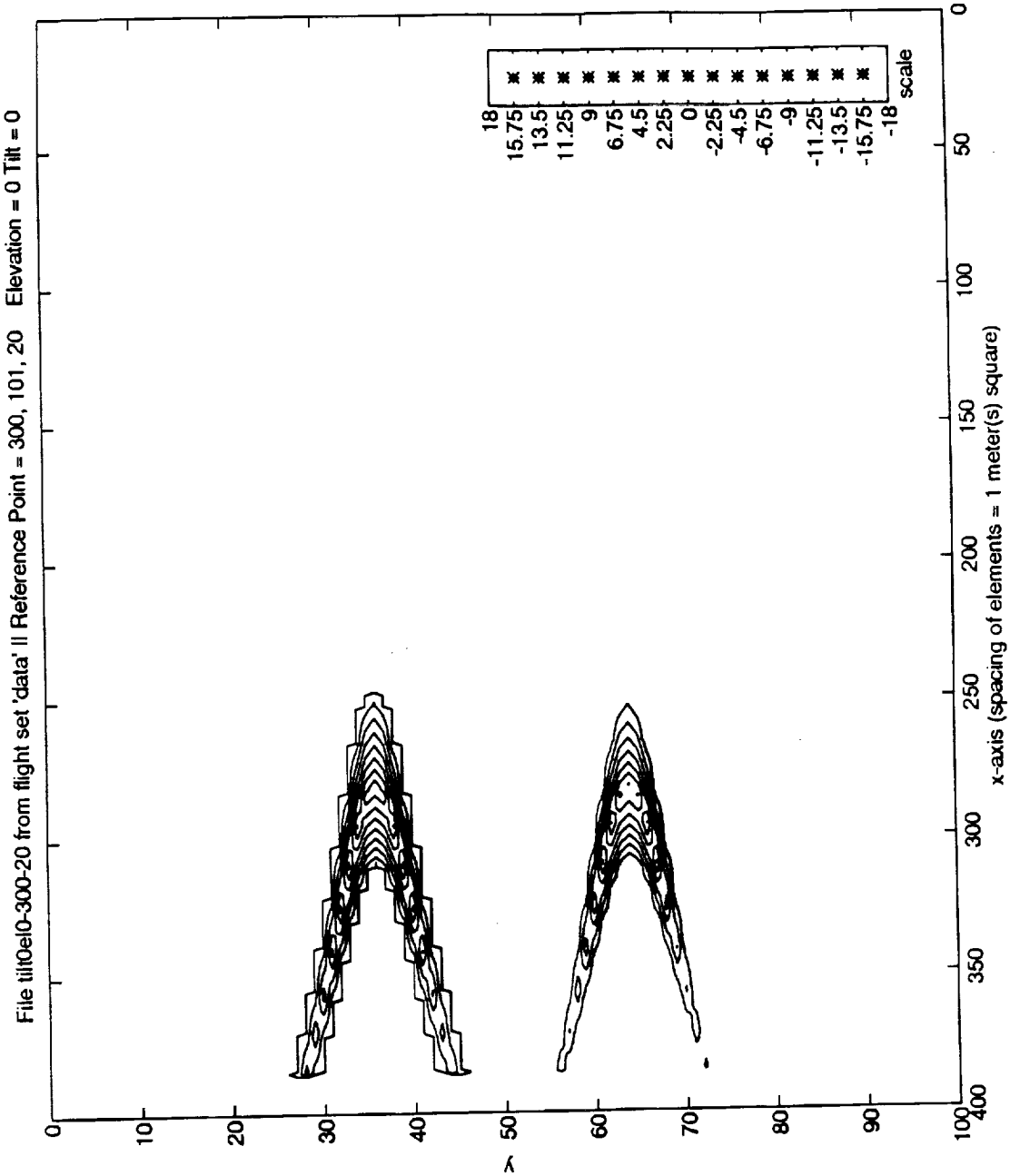
File tilt0el0-300-20 from flight set 'data' II Reference Point = 300, 101, 20 Elevation = 0 Tilt = 0
scale
18
15.75
13.5
11.25
9
6.75
4.5
2.25
0
-2.25
-4.5
-6.75
-9
-11.25
-13.5
-15.75
-18
y
x-axis (spacing of elements = 1 meter(s) square)
0
10
20
30
40
50
60
70
80
90
100
0
50
100
150
200
250
300
350
400

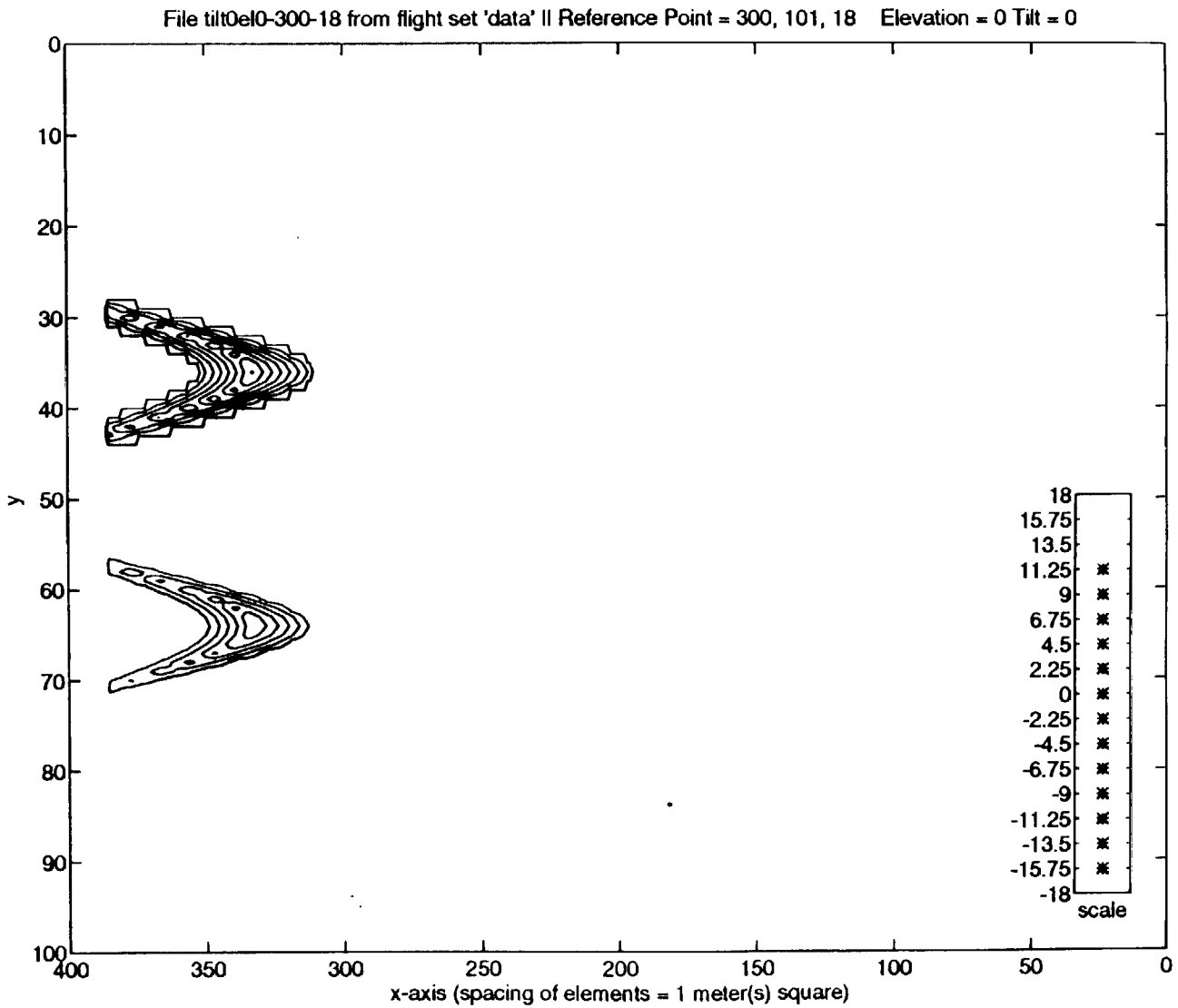
File tilt0el0-300-18 from flight set 'data' || Reference Point = 300, 101, 18 Elevation = 0 Tilt = 0
y
x-axis (spacing of elements = 1 meter(s) square)
scale
18
15.75
13.5
11.25
9
6.75
4.5
2.25
0
-2.25
-4.5
-6.75
-9
-11.25
-13.5
-15.75
-18

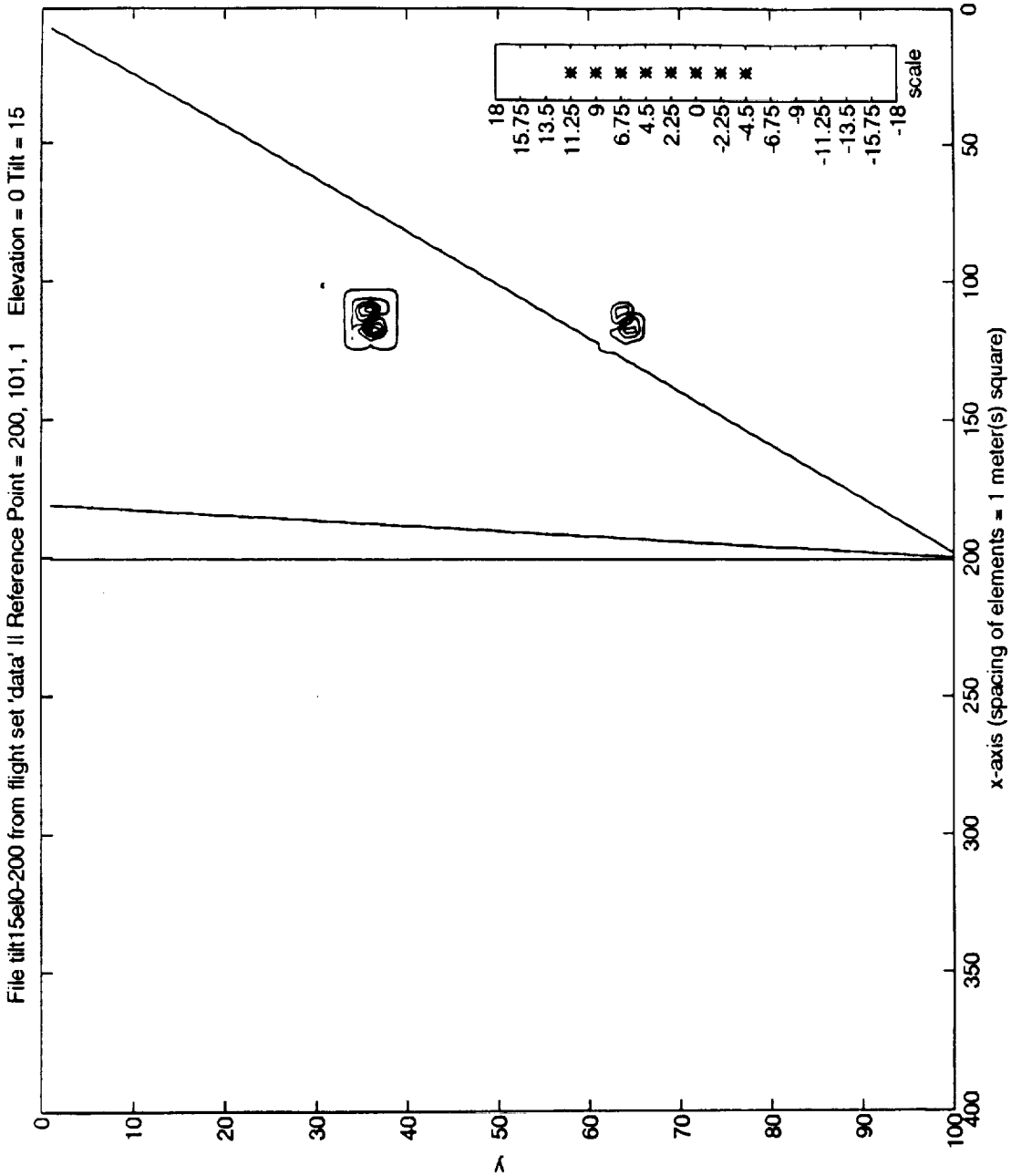
File tilt15el0-200 from flight set 'data' II Reference Point = 200, 101, 1 Elevation = 0 Tilt = 15
x-axis (spacing of elements = 1 meter(s) square)
y
scale
18
15.75
13.5
11.25
9
6.75
4.5
2.25
0
-2.25
-4.5
-6.75
-9
-11.25
-13.5
-15.75
-18
0
50
100
150
200
250
300
350
400
10
20
30
40
50
60
70
80
90
100

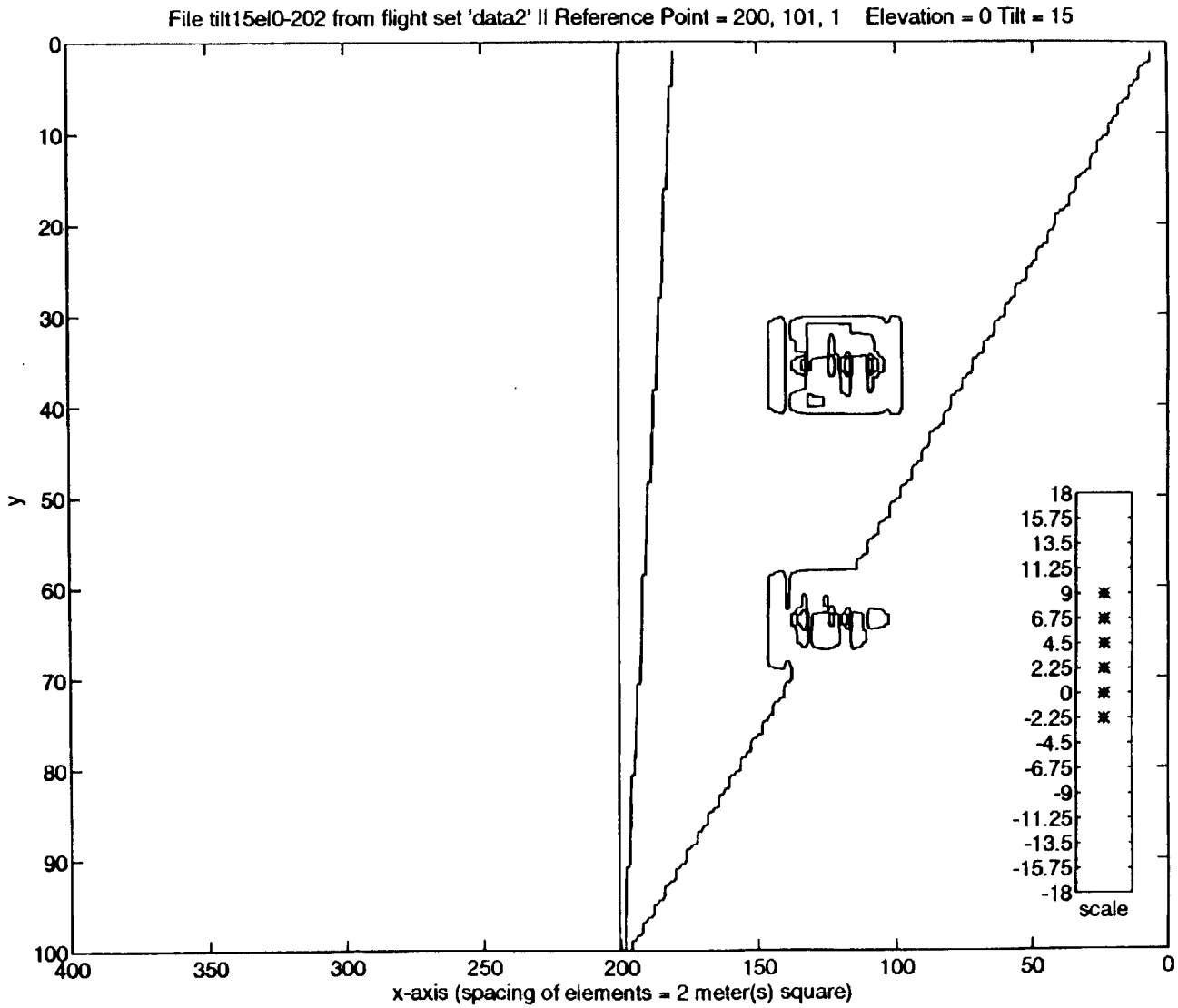
File tilt15el0-202 from flight set 'data2' II Reference Point = 200, 101, 1 Elevation = 0 Tilt = 15
y
x-axis (spacing of elements = 2 meter(s) square)
scale
18
15.75
13.5
11.25
9
6.75
4.5
2.25
0
-2.25
-4.5
-6.75
-9
-11.25
-13.5
-15.75
-18

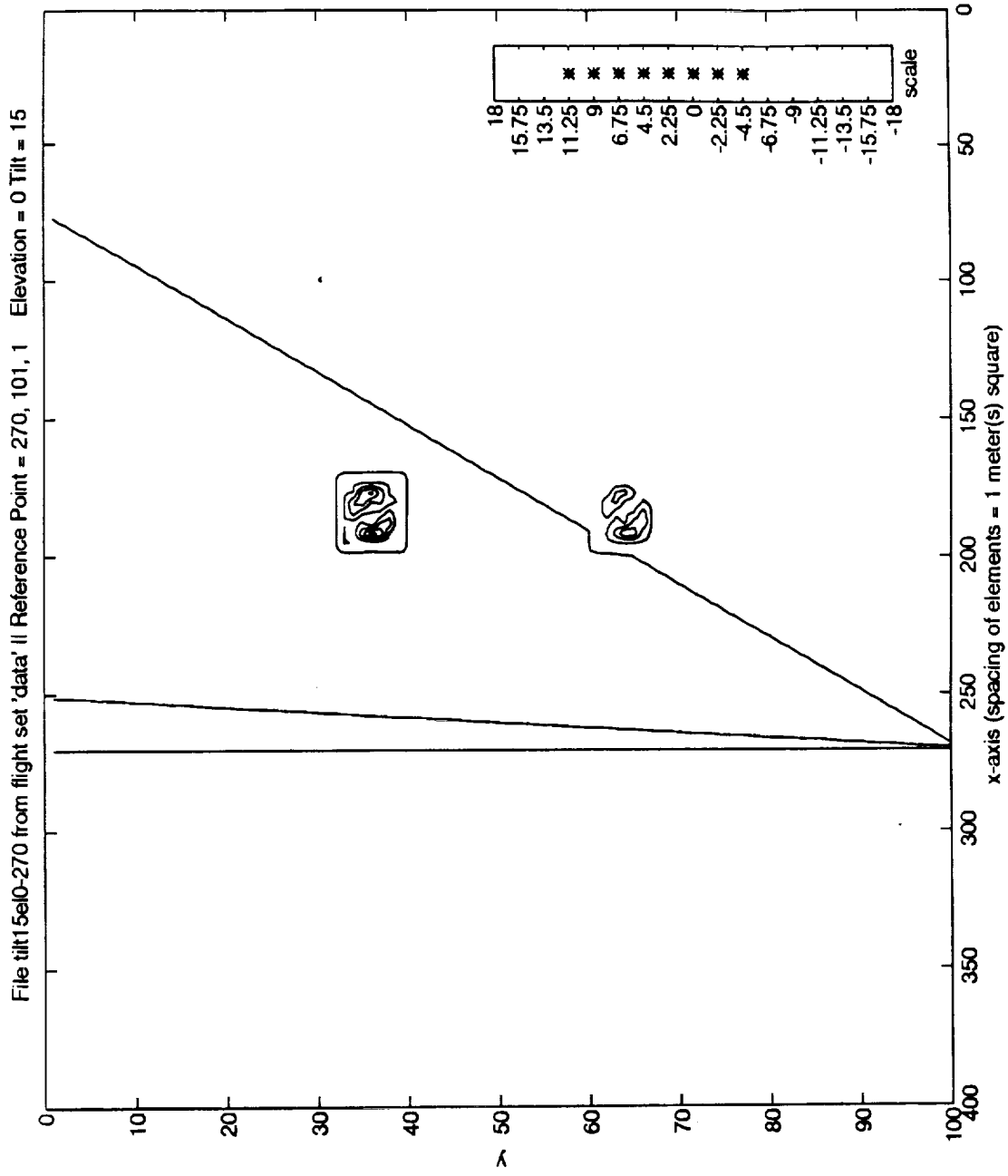
File tilt15el0-270 from flight set 'data' II Reference Point = 270, 101, 1 Elevation = 0 Tilt = 15
x-axis (spacing of elements = 1 meter(s) square)
y
scale
18
15.75
13.5
11.25
9
6.75
4.5
2.25
0
-2.25
-4.5
-6.75
-9
-11.25
-13.5
-15.75
-18
0
10
20
30
40
50
60
70
80
90
100
0
50
100
150
200
250
300
350
400

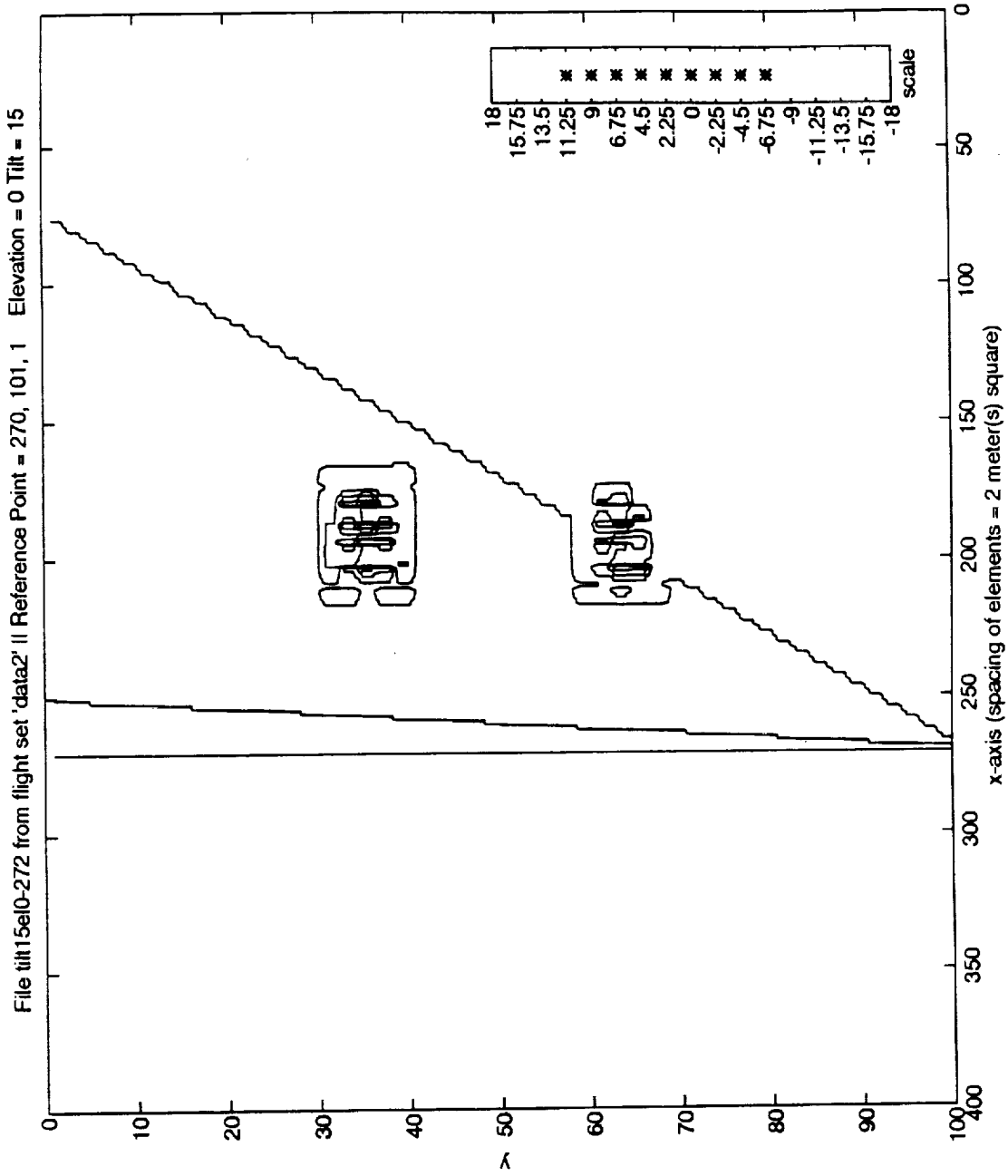
File tilt15el0-272 from flight set 'data2' II Reference Point = 270, 101, 1 Elevation = 0 Tilt = 15
scale
18
15.75
13.5
11.25
9
6.75
4.5
2.25
0
-2.25
-4.5
-6.75
-9
-11.25
-13.5
-15.75
-18
y
x-axis (spacing of elements = 2 meter(s) square)
0
10
20
30
40
50
60
70
80
90
100
0
50
100
150
200
250
300
350
400

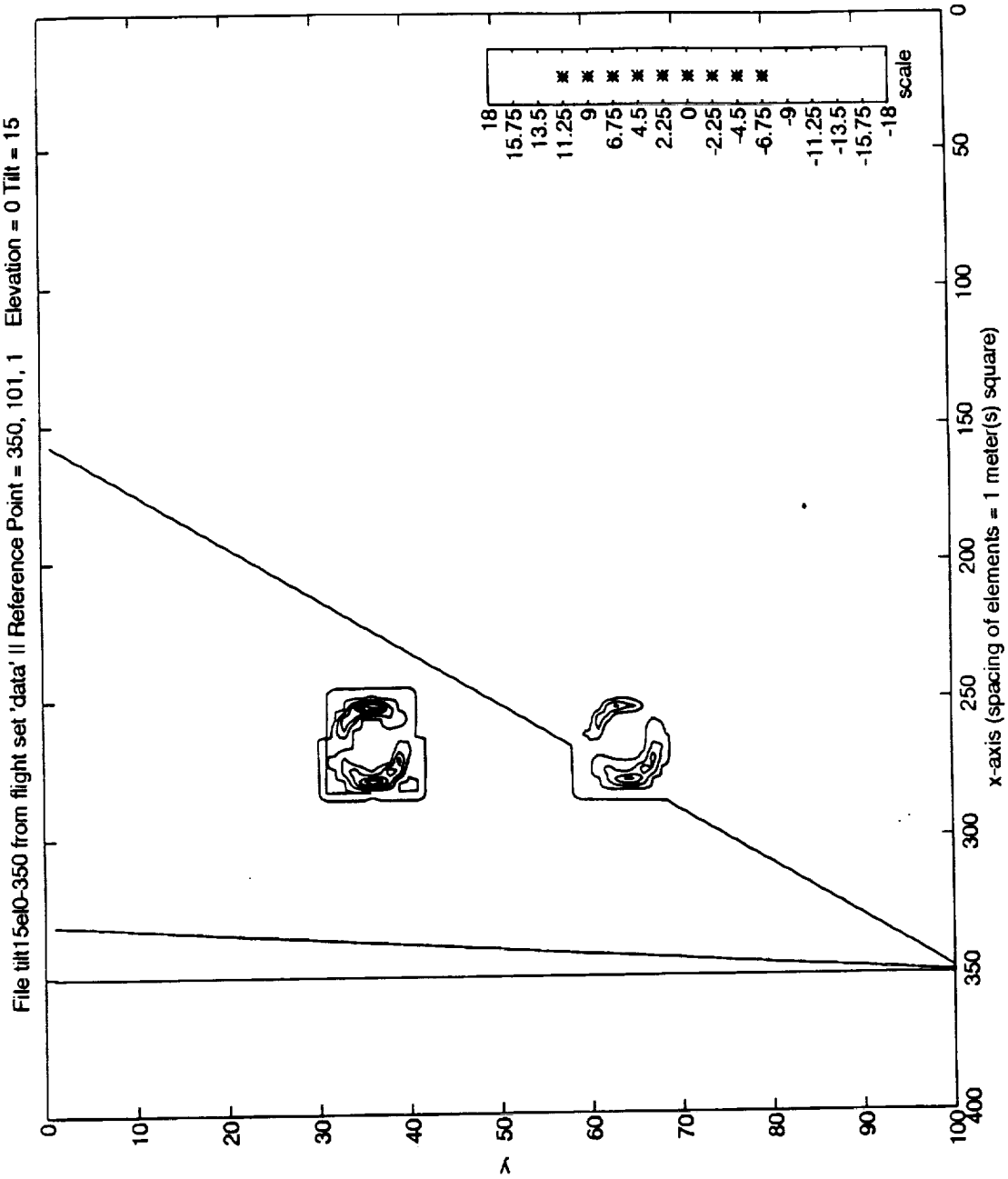
File tilt15el0-350 from flight set 'data' II Reference Point = 350, 101, 1 Elevation = 0 Tilt = 15
x-axis (spacing of elements = 1 meter(s) square)
Y
scale
18
15.75
13.5
11.25
9
6.75
4.5
2.25
0
-2.25
-4.5
-6.75
-9
-11.25
-13.5
-15.75
-18
0
50
100
150
200
250
300
350
400
0
10
20
30
40
50
60
70
80
90
100

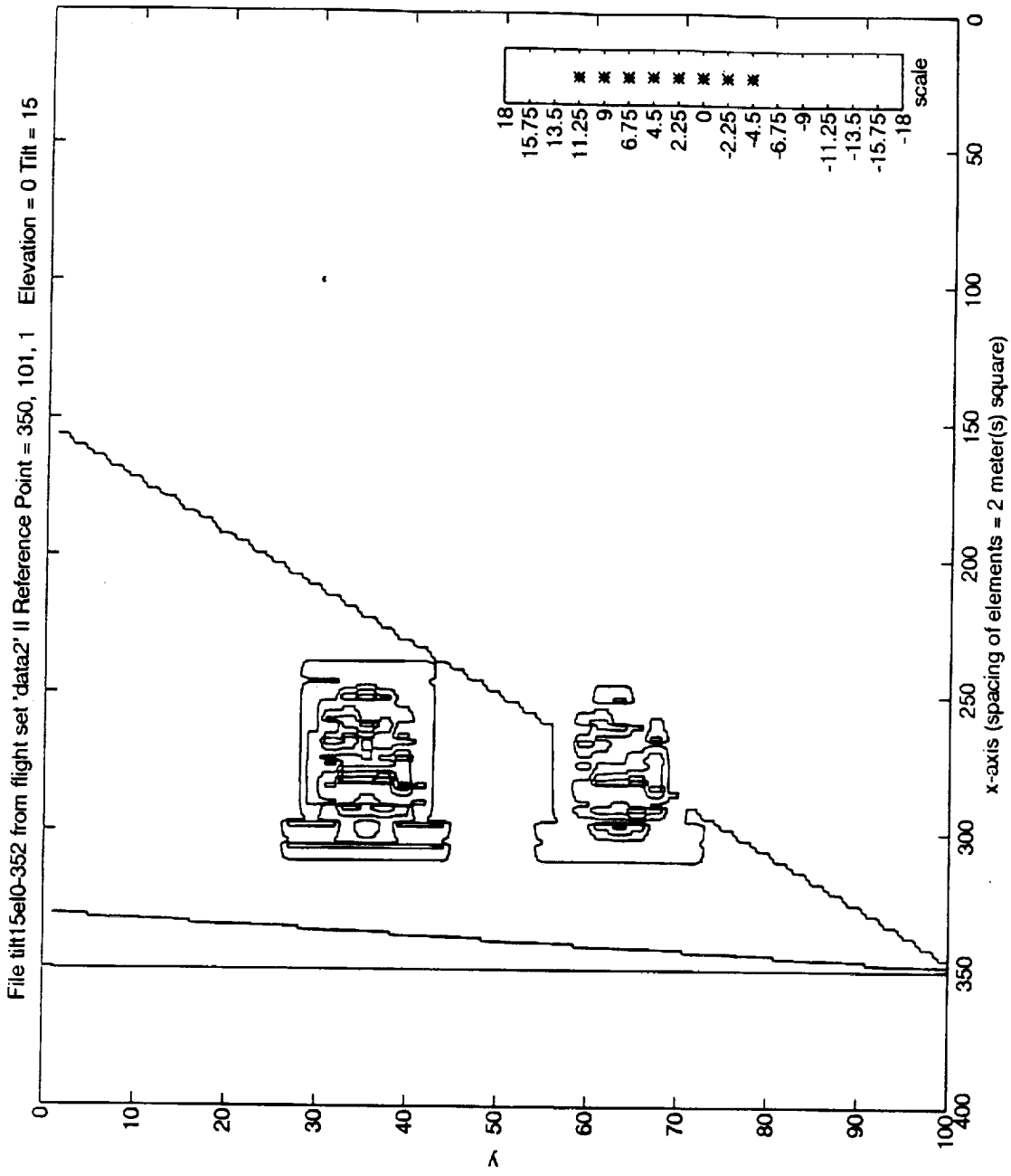
File tilt15el0-352 from flight set 'data2' II Reference Point = 350, 101, 1 Elevation = 0 Tilt = 15
scale
18
15.75
13.5
11.25
9
6.75
4.5
2.25
0
-2.25
-4.5
-6.75
-9
-11.25
-13.5
-15.75
-18
Y
x-axis (spacing of elements = 2 meter(s) square)

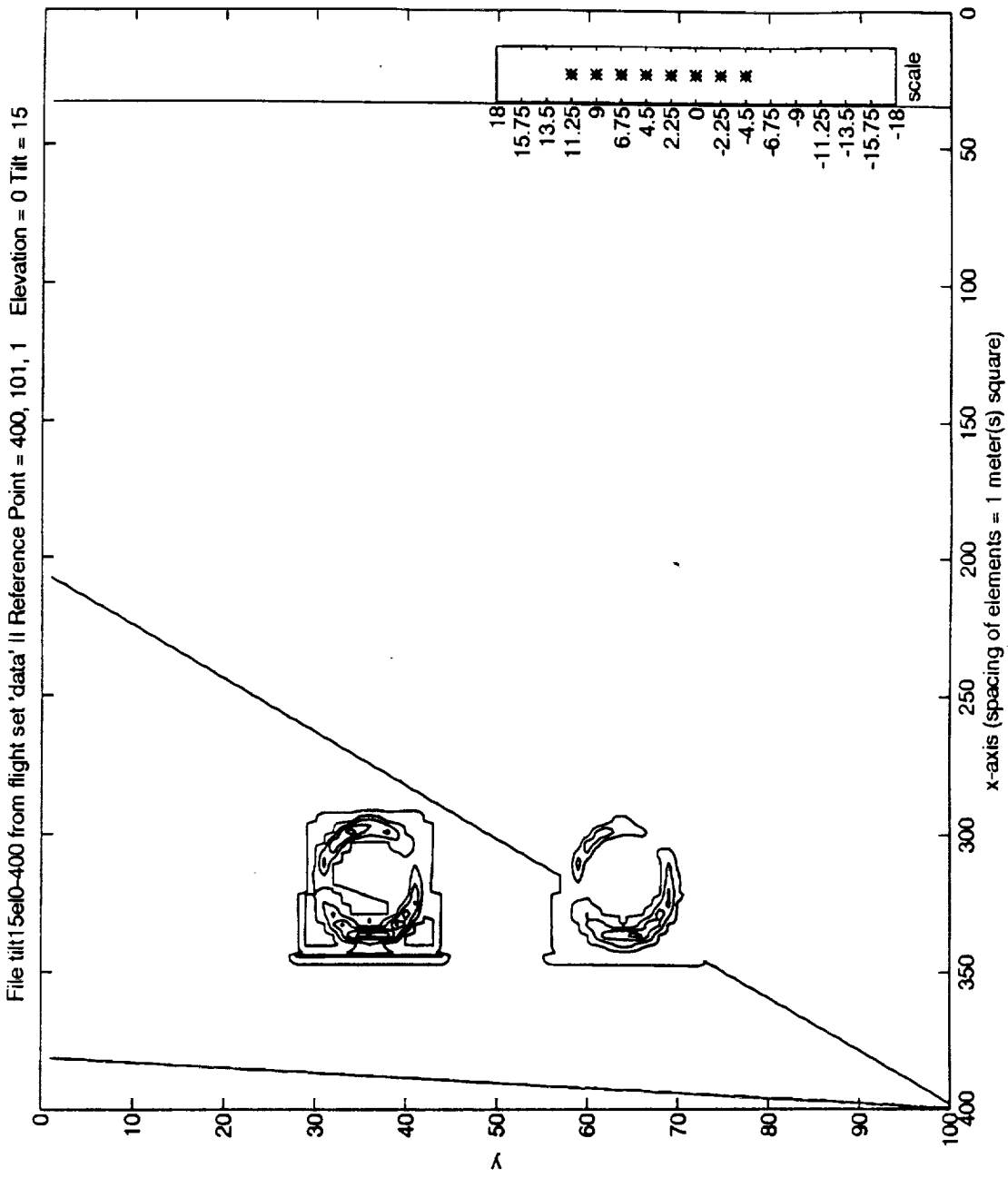
File tilt15el0-400 from flight set 'data' II Reference Point = 400, 101, 1 Elevation = 0 Tilt = 15
scale
18
15.75
13.5
11.25
9
6.75
4.5
2.25
0
-2.25
-4.5
-6.75
-9
-11.25
-13.5
-15.75
-18
y
x-axis (spacing of elements = 1 meter(s) square)

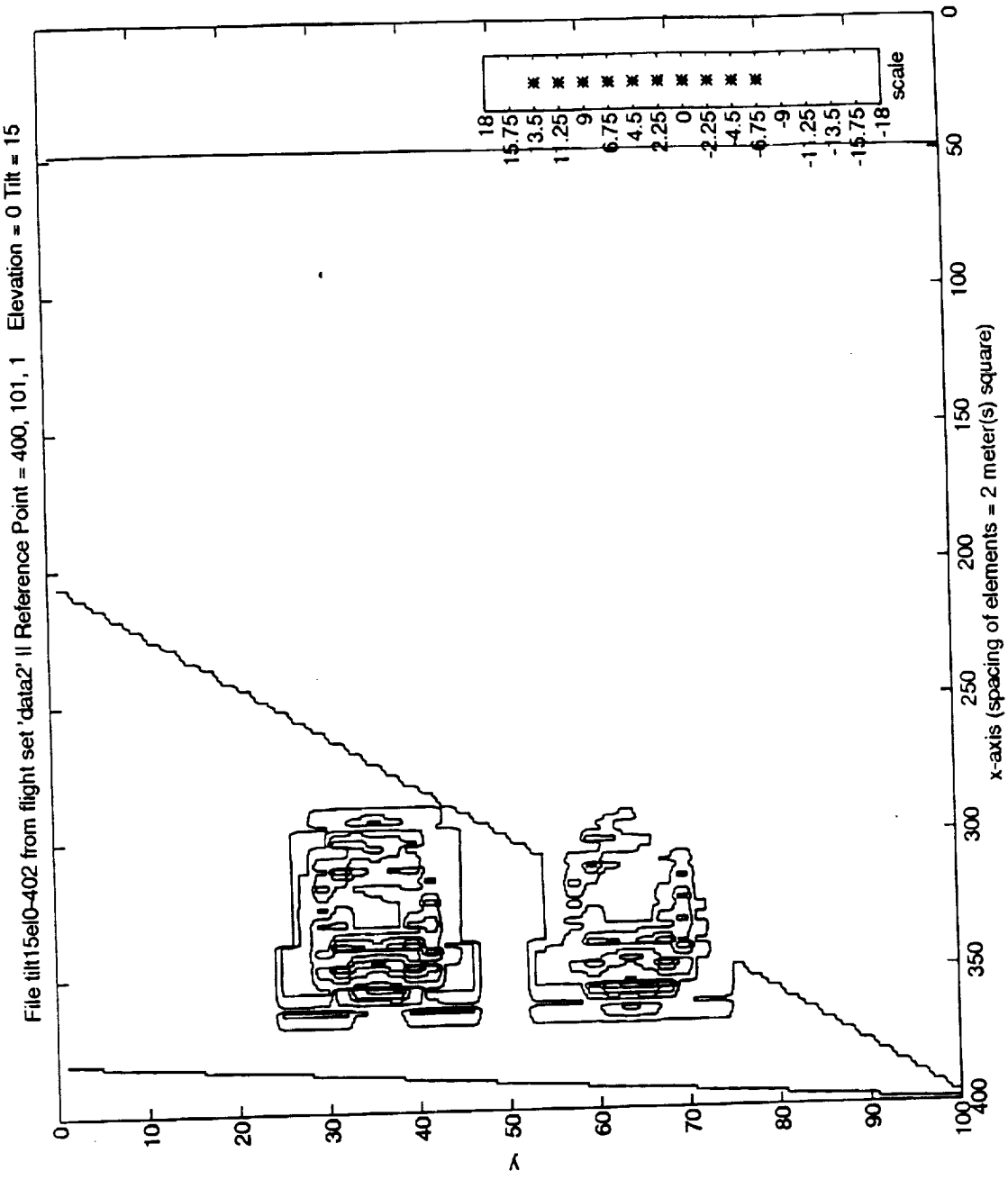
File tilt15el0-402 from flight set 'data2' II Reference Point = 400, 101, 1 Elevation = 0 Tilt = 15
scale
18
15.75
13.5
11.25
9
6.75
4.5
2.25
0
-2.25
-4.5
-6.75
-9
-11.25
-13.5
-15.75
-18
Y
0
10
20
30
40
50
60
70
80
90
100
0
50
100
150
200
250
300
350
400
x-axis (spacing of elements = 2 meter(s) square)

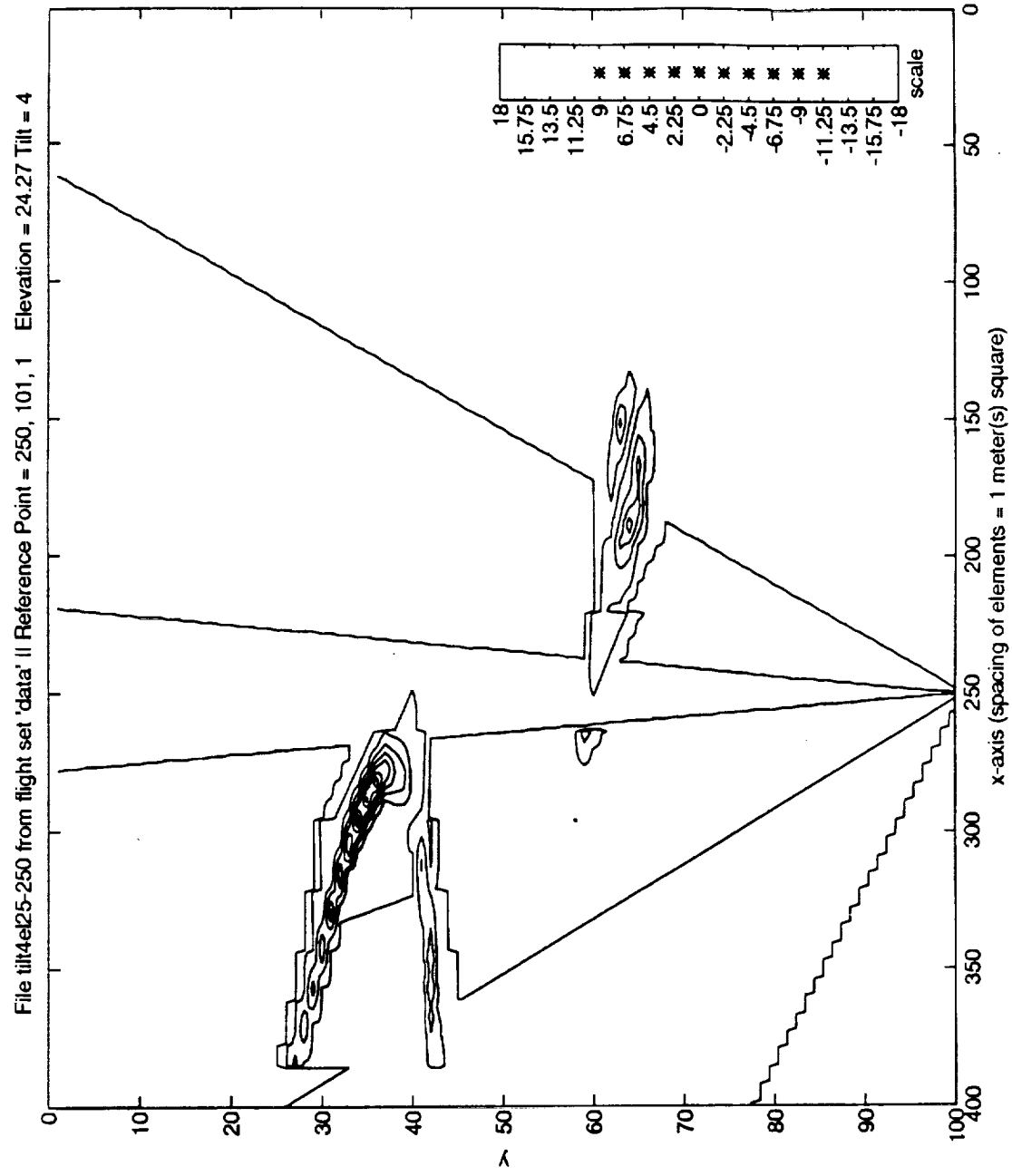
File tilt4el25-250 from flight set 'data' || Reference Point = 250, 101, 1 Elevation = 24.27 Tilt = 4
scale
18
15.75
13.5
11.25
9
6.75
4.5
2.25
0
-2.25
-4.5
-6.75
-9
-11.25
-13.5
-15.75
-18
y
x-axis (spacing of elements = 1 meter(s) square)
0
10
20
30
40
50
60
70
80
90
100
0
50
100
150
200
250
300
350
400

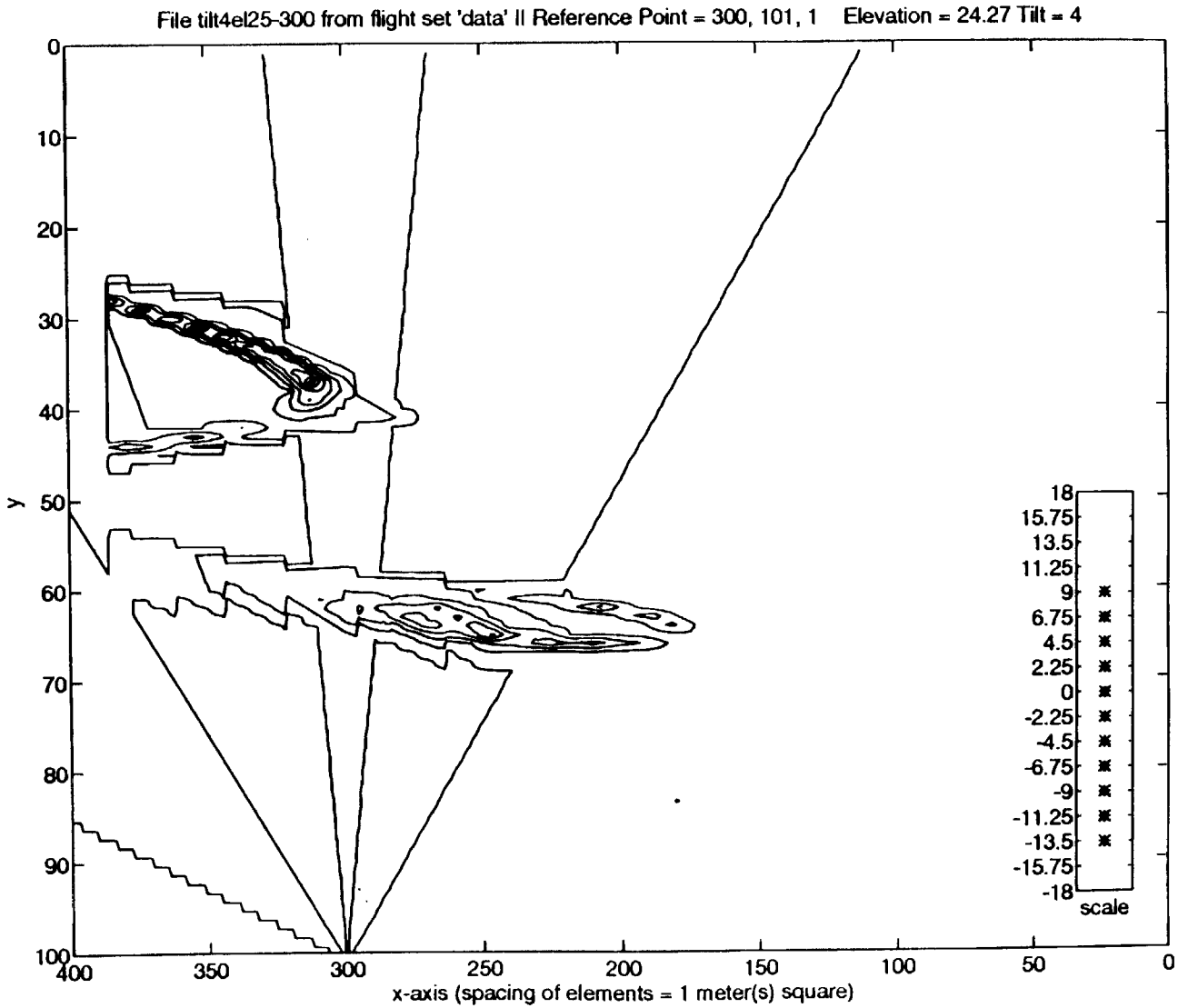
File tilt4el25-300 from flight set 'data' II Reference Point = 300, 101, 1 Elevation = 24.27 Tilt = 4
y
x-axis (spacing of elements = 1 meter(s) square)
scale
18
15.75
13.5
11.25
9
6.75
4.5
2.25
0
-2.25
-4.5
-6.75
-9
-11.25
-13.5
-15.75
-18
0
10
20
30
40
50
60
70
80
90
100
400
350
300
250
200
150
100
50
0

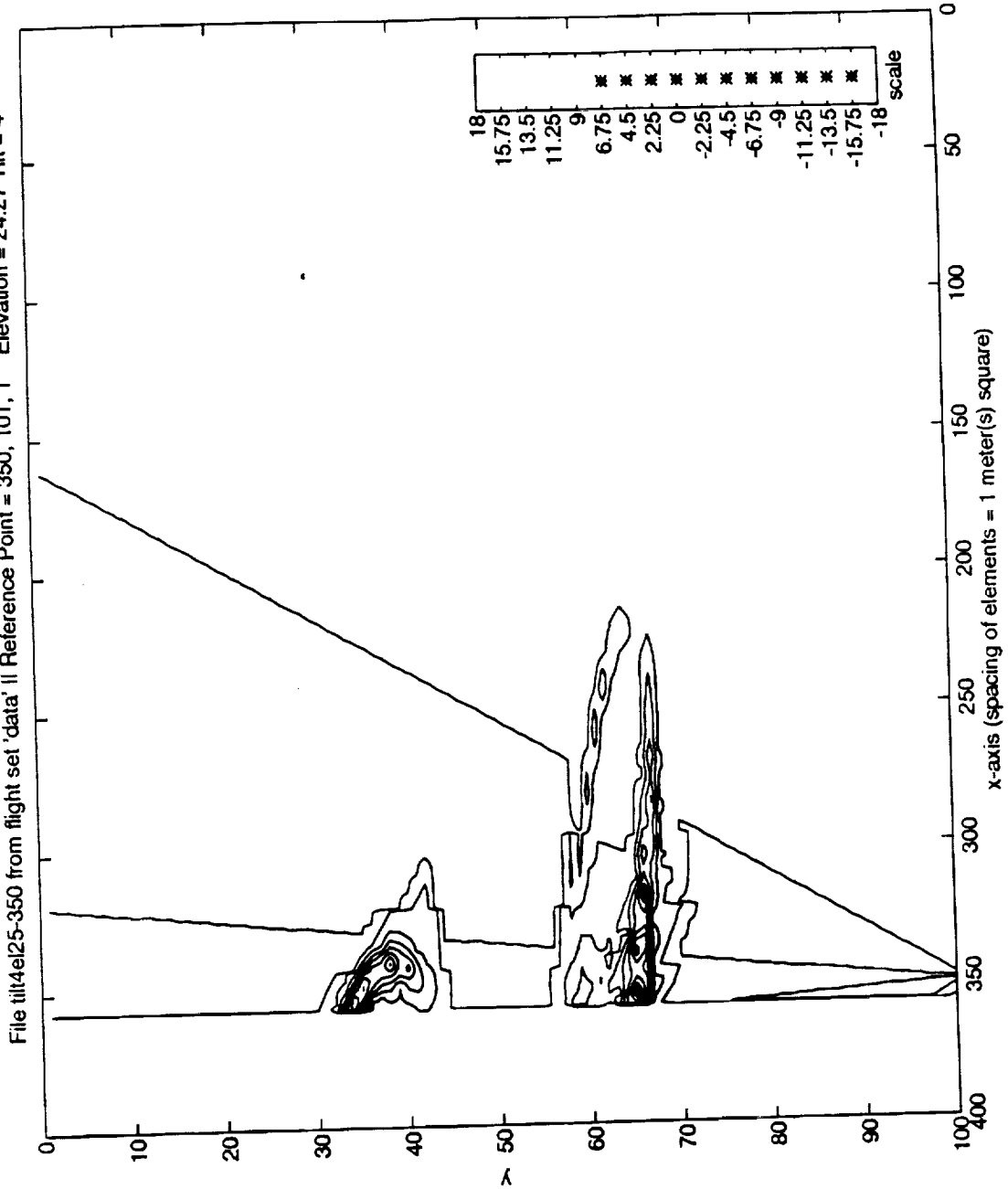
File tilt4el25-350 from flight set 'data' II Reference Point = 350, 101, 1 Elevation = 24.27 Tilt = 4
x-axis (spacing of elements = 1 meter(s) square)
Y
scale
18
15.75
13.5
11.25
9
6.75
4.5
2.25
0
-2.25
-4.5
-6.75
-9
-11.25
-13.5
-15.75
-18

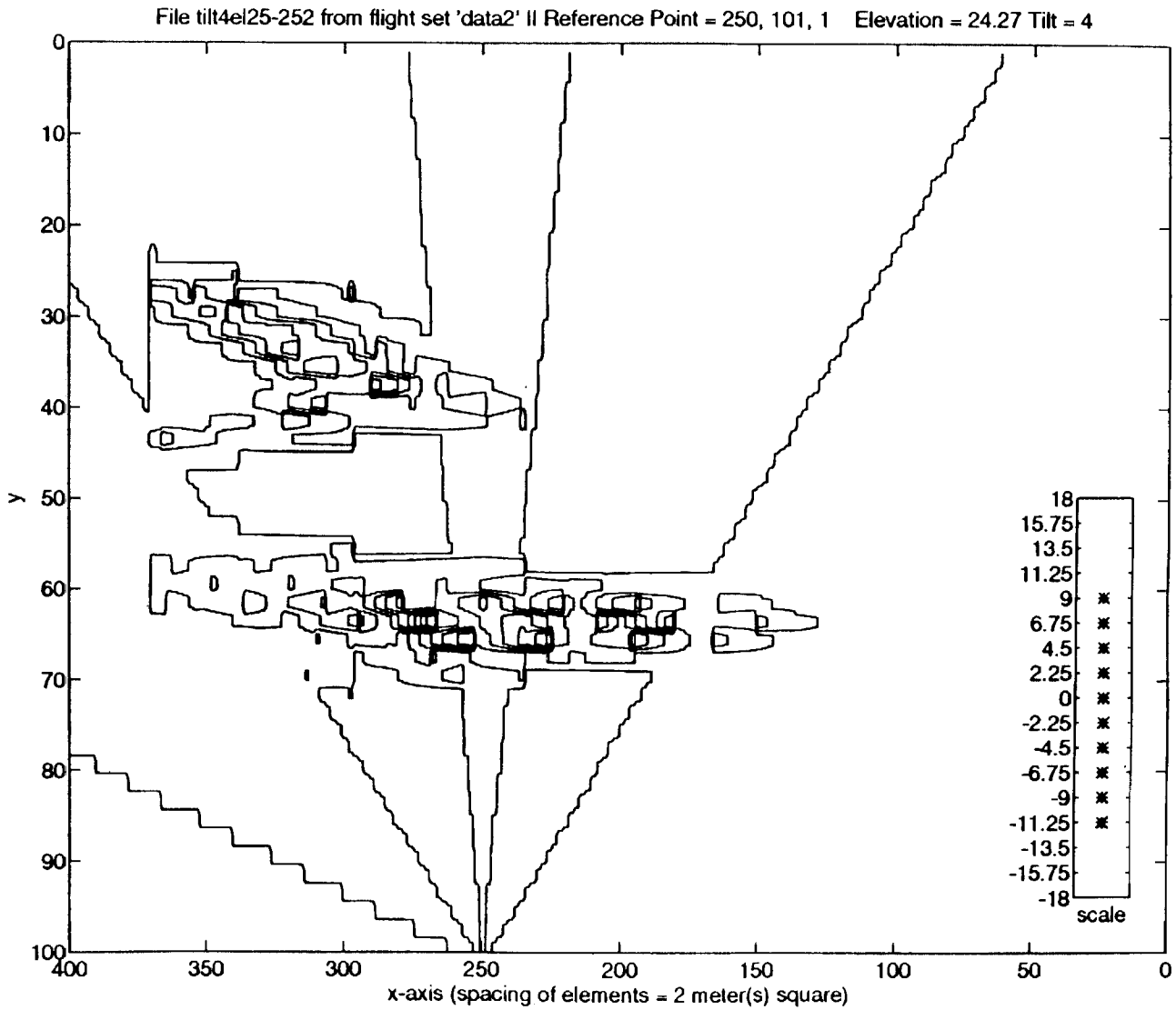
File tilt4el25-252 from flight set 'data2' II Reference Point = 250, 101, 1 Elevation = 24.27 Tilt = 4
y
x-axis (spacing of elements = 2 meter(s) square)
0
10
20
30
40
50
60
70
80
90
100
400
350
300
250
200
150
100
50
0
18
15.75
13.5
11.25
9
6.75
4.5
2.25
0
-2.25
-4.5
-6.75
-9
-11.25
-13.5
-15.75
-18
scale

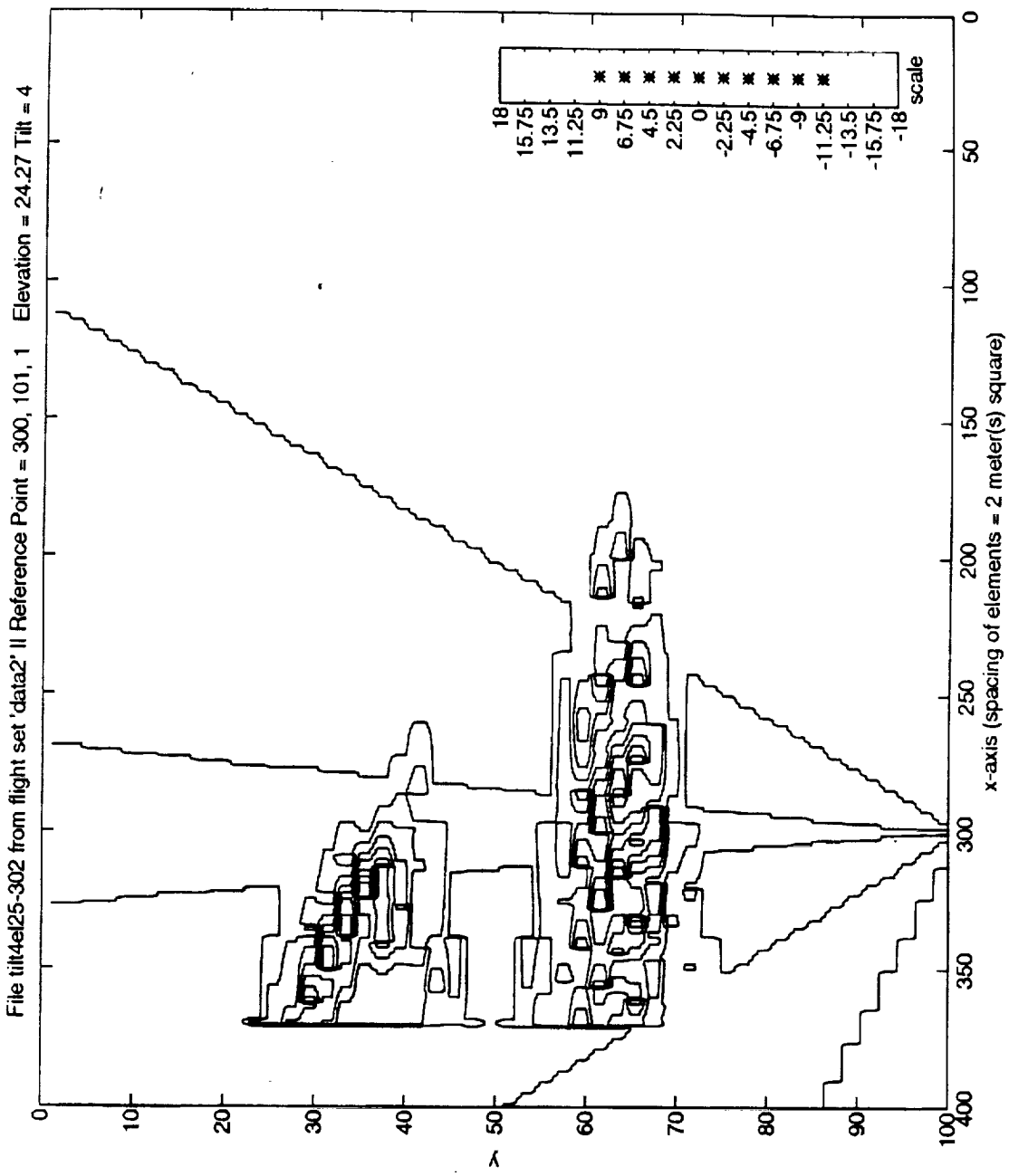
File tilt4el25-302 from flight set 'data2' II Reference Point = 300, 101, 1 Elevation = 24.27 Tilt = 4
x-axis (spacing of elements = 2 meter(s) square)
y
scale
18
15.75
13.5
11.25
9
6.75
4.5
2.25
0
-2.25
-4.5
-6.75
-9
-11.25
-13.5
-15.75
-18

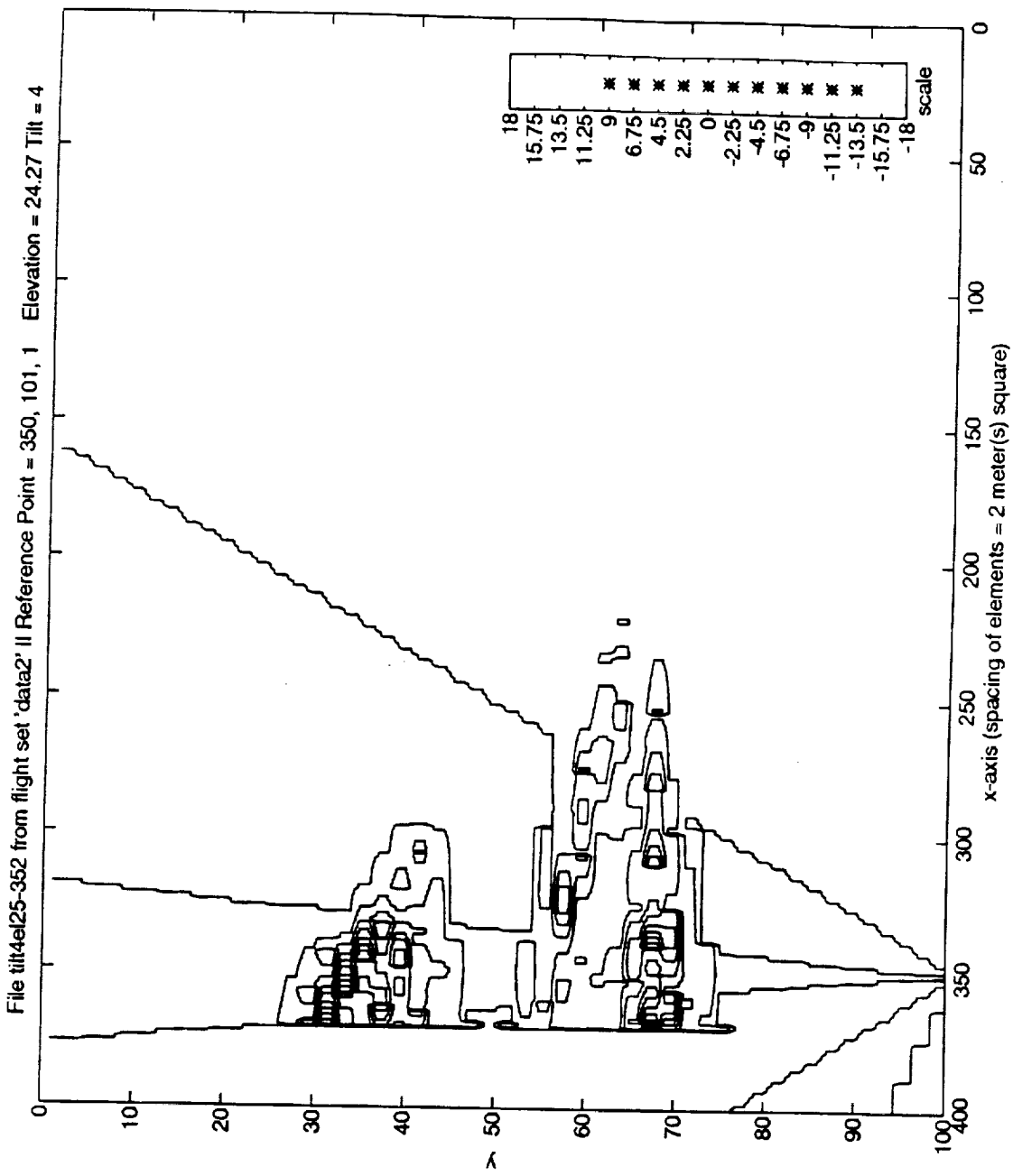
File tilt4el25-352 from flight set 'data2' II Reference Point = 350, 101, 1 Elevation = 24.27 Tilt = 4
18
15.75
13.5
11.25
9
6.75
4.5
2.25
0
-2.25
-4.5
-6.75
-9
-11.25
-13.5
-15.75
-18
scale
Y
x-axis (spacing of elements = 2 meter(s) square)

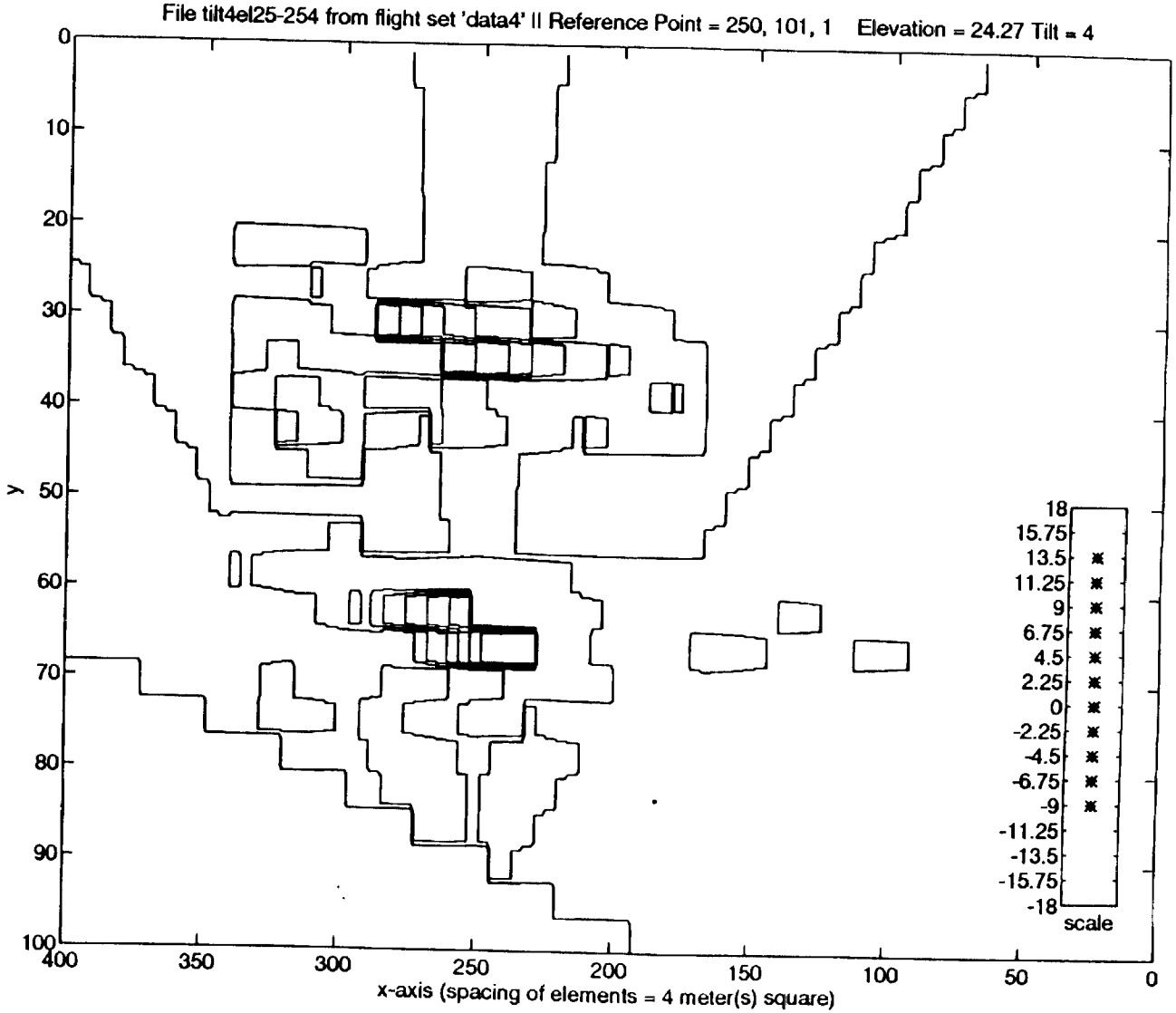
File tilt4el25-254 from flight set 'data4' || Reference Point = 250, 101, 1 Elevation = 24.27 Tilt = 4
y
x-axis (spacing of elements = 4 meter(s) square)
scale
18
15.75
13.5
11.25
9
6.75
4.5
2.25
0
-2.25
-4.5
-6.75
-9
-11.25
-13.5
-15.75
-18

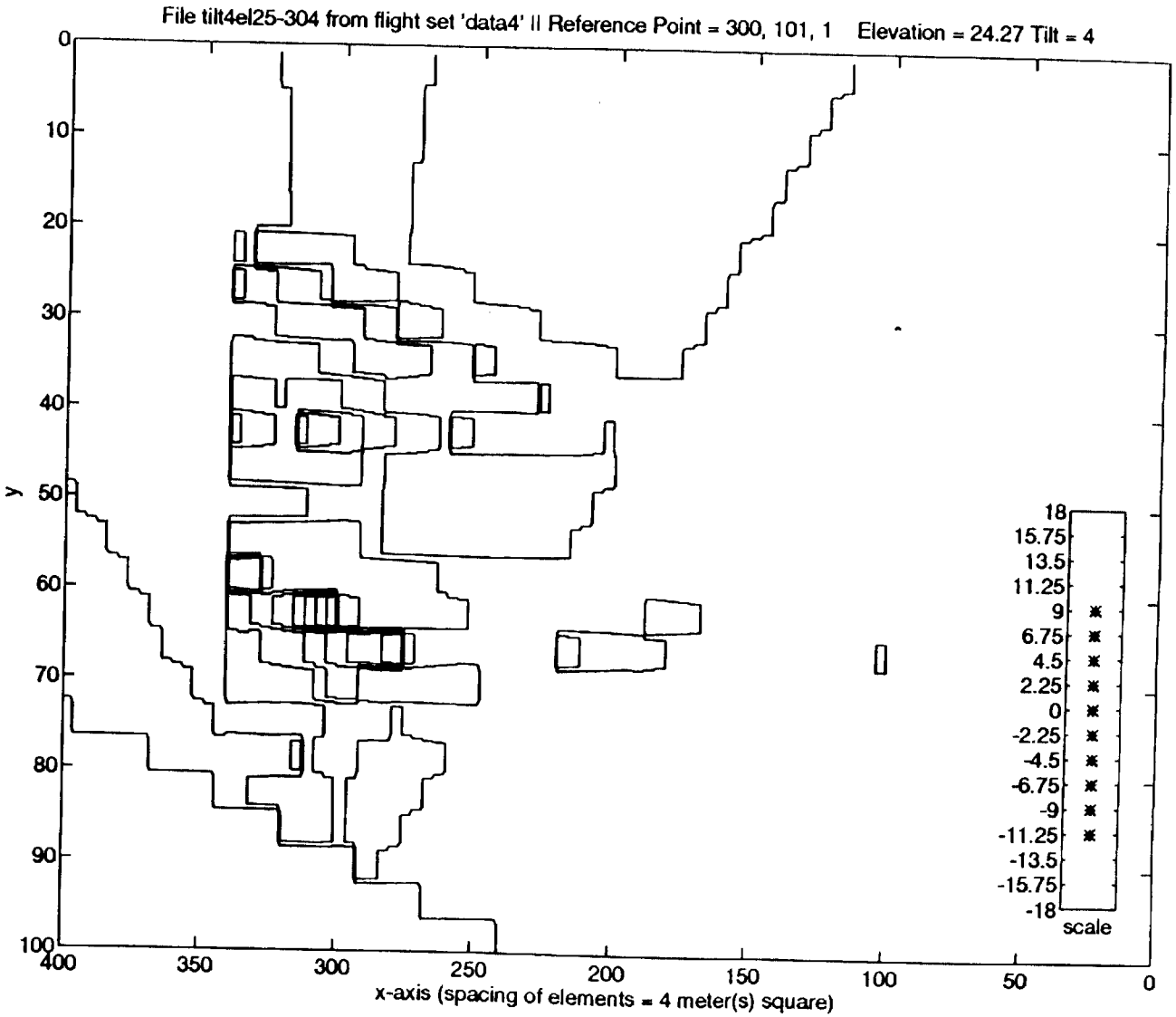
File tilt4el25-304 from flight set 'data4' II Reference Point = 300, 101, 1 Elevation = 24.27 Tilt = 4
y
x-axis (spacing of elements = 4 meter(s) square)
scale
18
15.75
13.5
11.25
9
6.75
4.5
2.25
0
-2.25
-4.5
-6.75
-9
-11.25
-13.5
-15.75
-18
0
10
20
30
40
50
60
70
80
90
100
400
350
300
250
200
150
100
50
0

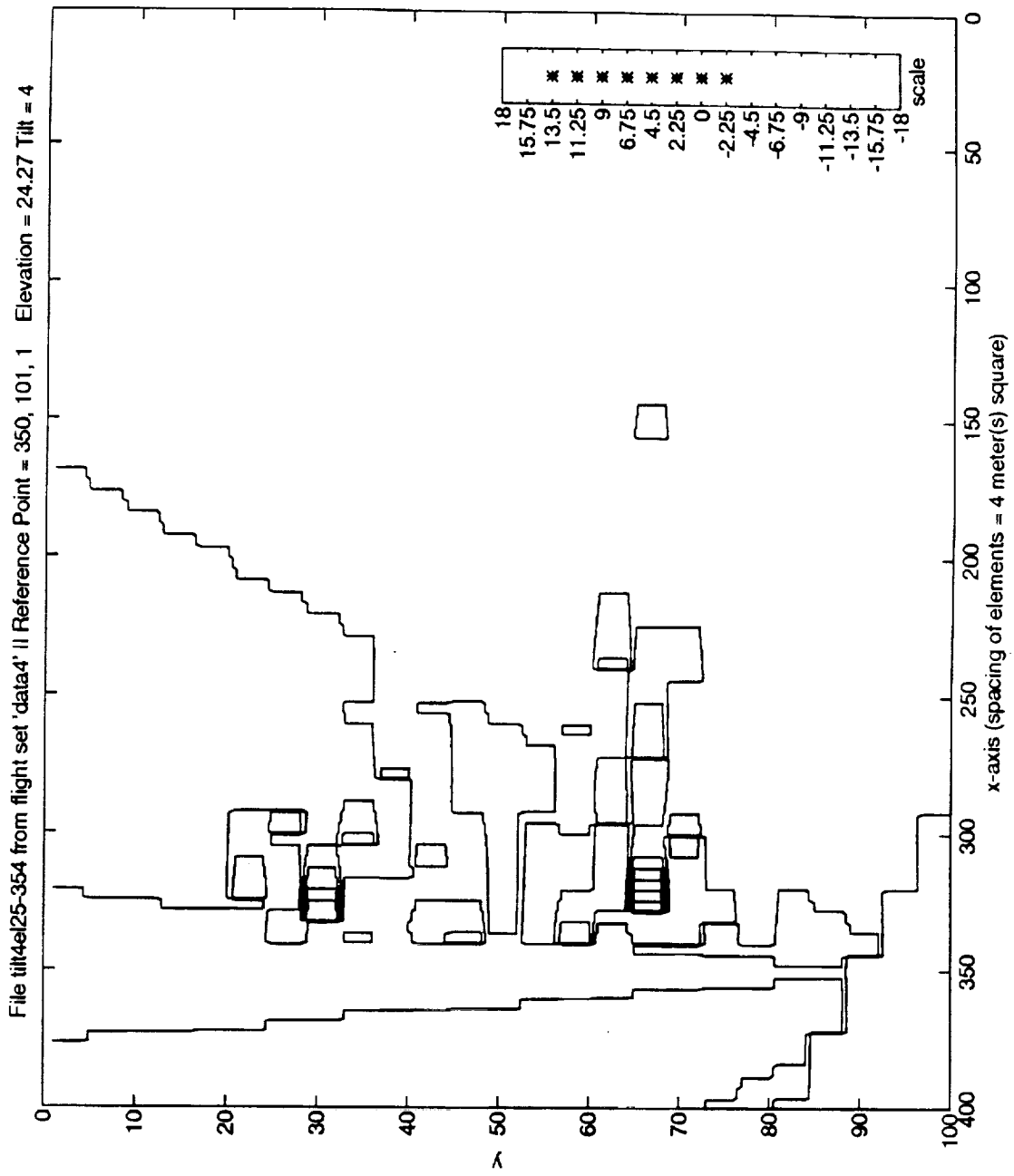
File tilt4el25-354 from flight set 'data4' II Reference Point = 350, 101, 1 Elevation = 24.27 Tilt = 4
x-axis (spacing of elements = 4 meter(s) square)
Y
scale
18
15.75
13.5
11.25
9
6.75
4.5
2.25
0
-2.25
-4.5
-6.75
-9
-11.25
-13.5
-15.75
-18

REFERENCES

1. G. V. Morris, editor. *Airborne Pulsed Doppler Radar.* Artech House, Norwood, Massachusetts, 1988.

2. E. G. Baxa, Jr. "Airborne Pulsed Doppler Radar Detection of Low-Altitude Windshear — A Signal Processing Problem". *Digital Signal Processing,* 1(4):186–197, October 1991.

3. E. G. Baxa, Jr. and J. Lee. "The Pulse Pair Algorithm as a Robust Estimator of Turbulent Weather Spectral Parameters Using Airborne Pulse Doppler Radar". NASA CR–186792, February 1991.

4. M. I. Skolnik, editor. *Radar Handbook.* McGraw–Hill, New York, 1990.

5. Garrett Birkhoff and E.H. Zarantonello, editors. *Jets, Wakes and Cavaties.* Academic Press Inc., New York, 1957.

6. Hans J. Lugt, editor. *Vortex Flow in Nature and Technology.* John Wiley and Sons, New York, 1983.

7. Steven Vogel. " Life in a Whirl. (The Vortex in Nature)". *Discover,* pages 80–86, August 1993.

8. C. Anderson and C. Greengard. "Lecture Notes in Mathematics: Vortex Methods". Proceedings of the U.C.L.A. Workshop, Los Angeles, California, May 20 - 22, 1987.

9. Robert E. Marshall, Mark A. Richards, Joe A. Galliano, and Jorge Montoya. "Advanced Microwave Sensing Technology Study for Civil Aviation Atmospheric Hazards". Tech. Memo. Project NAS1 - 18925, Research Triangle Institute and Georgia Tech Research Institute, Research Triangle Park, North Carolina, November 1992.

10. S. Goldstein, editor. *Modern Developments in Fluid Dynamics.* Clarendon Press, Oxford, 1938.

11. Peter Lert. "Stay Awake and Alive". *Air Progress,* pages 4,32–33,56, March 1994.

12. Mark Lambert, editor. *Jane's All the World's Aircraft.* Butler and Tanner Ltd., Allendale, Virginia, 1993.